Development of Aqueous CdS and CdTe/CdS Quantum Dots via DMSA decomposition

by

ESRA SEVİNÇ

A Thesis Submitted to the
Graduate School of Sciences and Engineering
in Partial Fulfillment of the Requirements for
the Degree of

Master of Science
in
Materials Science and Engineering

Koc University

August 2009

Koc University

Graduate School of Sciences and Engineering

This is to certify that I have examined this copy of a master's thesis by

Esra Sevinç

and have found that it is complete and satisfactory in all respects,
and that any and all revisions required by the final
examining committee have been made.

Committee Members:

_____

Havva Funda Yağcı Acar, Ph. D. (Advisor)

_____

Mehmet Suat Somer, Ph. D.

_____

Alphan Sennaroğlu, Ph. D.

Date: _____

ABSTRACT

Quantum dots (QDs) have attracted great interest and gained significance in many research areas of science and technology due to their unique chemical and physical properties. The most striking property of these semiconductor nanocrystals is the size-dependent absorbance and emission spectra as a result of quantum confinement. Moreover, they have high quantum efficiencies, narrow and symmetric emission spectrum, wide optical absorption bands, long fluorescence lifetime in comparison with organic fluorophores and compatibility with organic solvents and biological media. This M.S. thesis mostly concerns about the applications of quantum dots in biotechnology and medicine.

The research of this thesis aims at developing highly luminescent, colloidal aqueous quantum dots which are applicable to biological systems. In order to achieve this goal, DMSA (meso-2,3-dimercaptosuccinic acid) was chosen as the stabilizer (surfactant), which is known to be bio-compatible. In the first step, CdS QDs were prepared by a very simple experimental strategy. Effects of reaction temperature, pH and DMSA amount on particle size and quantum yield (QY) were examined. As a result, DMSA was used both as a stabilizer and a sulphur source in the synthesis of colloidal, highly stable aqueous CdS QDs. Particles luminescing from blue to orange with QY values of 8-10 % were obtained at pH 7.5 and 70ºC. In these syntheses, SH (DMSA)/Cd ratio of 2.7 was determined as the optimum ratio providing highest QY.

The second step was the fabrication of 2-mercaptopropionic acid (2-MPA) capped CdTe/CdS core/shell QDs by the decomposition of DMSA. The shell growth improved the optical quality of CdTe core significantly. Three important reaction parameters (SH(DMSA)/Cd ratio, initial pH and SH(2-MPA)/Cd ratio) were investigated. Consequently, CdTe/CdS core/shell QDs luminescing from green to red were accomplished

with a maximum QY of 73.3% by the decomposition of DMSA without any post-preparative method. Optimum reaction conditions were initial pH of 7.5, Cd^{2+}:Te^{2-}:SH(2-MPA) ratio of 1:0.38:2.4 and Cd^{2+}:SH(DMSA) ratio of 1:0.7. Besides, DMSA was compared with a common sulphur source, thioacetamide (TAA), and much better luminescence compared to TAA case was obtained with the DMSA. Results indicate that DMSA acts both as a sulfur source for the shell growth and as a co-surfactant which improved both optical properties and long-term stability of particles. Shell growth removes surface defects and therefore radiative coupling events were supported. This is shown by increasing luminescence lifetimes (both short and long-lifetime components) and increasing weight of the surface related emission lifetime values.

Overall, the research summarized in this thesis elucidates the dual action of DMSA (capping agent and sulfur source) in CdS QD synthesis and further proves the effectiveness of DMSA in the formation of colorful, stable and highly luminescent CdTe/CdS core/shell QDs. Considering the simplicity of the synthesis method and the biocompatibility of DMSA, the information and materials prepared here should be valuable for biotechnology and medical research.

ÖZET

Kuantum noktacıkları, sahip oldukları eşsiz kimyasal ve fiziksel özelliklerinden dolayı bilim ve teknolojinin pek çok alanında büyük ilgi çekmiş ve önem kazanmıştır. Bu yarı iletken nano-parçacıkların en dikkat çeken özelliği kuantum sınırlamasının sonucunda ortaya çıkan büyüklüğe bağlı soğurma ve ışıma görüntüsüdür. Ayrıca, bunların yüksek kuantum verimi, dar ve simetrik ışıma spektrumu, geniş soğurma bandı, uzun ışınım ömrü ve organik çözücülere ve biyolojik otama uyumluluğu vardır. Bu yüksek mühendislik tezi ekseriyetle kuantum noktacıklarının biyoteknoloji ve tıp alanlarında uygulamalarıyla ilgilenmektedir.

Bu tezin araştırması yüksek derecede ışıyan, koloidal suda yapılan kuantum noktacıkların geliştirilmesini amaçlar ki bu noktacıklar biyolojik sistemlere uyumludurlar. Bu hedefi mümkün kılmak için biyo-uyumlu olarak bilinen DMSA (meso-2,3-dimerkapto süksinik asit) yüzey aktif madde (kaplayıcı) olarak seçilmiştir. İlk aşamada, çok basit bir deneysel yöntemle CdS kuantum noktacıkları üretilmiştir. Tepkime sıcaklığı, pH'ı ve DMSA miktarının parçacık büyüklüğüne ve kuantum verimine etkisi incelendi. Sonuç olarak, DMSA hem kaplayıcı hem de sülfür kaynağı olarak koloidal, yüksek derecede dayanıklı ve suda yapılan CdS kuantum noktacıklarının sentezinde kullanıldı. pH 7.5 ve 70ºC'de kuantum verimi %8-10 olan maviden turuncuya kadar ışıyan parçacıklar elde edildi. Bu sentezlerde, 2.7 olan SH (DMSA)/Cd oranı en yüksek kuantum verimini sağlayan en uygun oran olarak belirlendi.

İkinci aşama, DMSA'nın bozunumu sayesinde 2-merkapto propiyonik asit (2-MPA) kaplı CdTe/CdS merkez/kabuk kuantum noktacıkları üretilmesidir. Kabuk oluşması CdTe merkezinin optik kalitesini geliştirmiştir. Üç önemli tepkime parametresi (SH(DMSA)/Cd oranı, başlangıç pH'ı ve SH(2-MPA)/Cd oranı) incelendi. Sonuç olarak, tepkime sonrası hiçbir uygulamaya tabi tutulmadan, DMSA'nın bozunumu sayesinde, en yüksek %73.3

kuantum verimine sahip yeşilden kırmızıya kadar ışıyan CdTe/CdS merkez/kabuk kuantum noktacıkları elde edildi. Başlangıç pH'ı olarak 7.5, Cd^{2+}:Te^{2-}:SH(2-MPA) oranı olarak 1:0.38:2.4 ve Cd^{2+}:SH(DMSA) oranı olarak da 1:0.7, en uygun tepkime koşullarıydı. Bunun yanısıra, DMSA yaygın bir sülfür kaynağı olan tiyoasetamit (TAA) ile karşılaştırıldı ve DMSA sayesinde TAA durumundan çok daha iyi ışıma elde edildi. Sonuçlar gösterdi ki DMSA hem kabuk oluşması için sülfür kaynağı olarak görev aldı hem de yardımcı-kaplayıcı olarak parçacıkların optik özelliklerini ve uzun-dönem dayanıklılığını geliştirdi. Kabuk oluşması yüzeydeki bozuklukları ortadan kaldırır ve bu sayede ışımayı sağlayan bağlantılar desteklenir. Bu durum ışıma ömrünün (hem kısa hem de uzun-dönem ışıma ömrü bileşenlerinin) artması ve yüzeyle alakalı ışıma ömrünün yüzde ağırlığının artması ile gösterilmiştir.

Sonuç olarak, bu tezde özetlenen araştırma, DMSA'nın ikili özelliğinin (kaplayıcı ve sülfür kaynağı) CdS kuantum noktacığı sentezinde kullanıldığını anlatmaktadır ve hatta DMSA'nın rengârenk, dayanıklı ve yüksek derecede ışıyan CdTe/CdS merkez/kabuk kuantum noktacıklarının oluşmasındaki etkisi kanıtlamıştır. Sentez yönteminin basitliği ve DMSA'nın biyo-uyumluluğu göz önüne alındığında, burada belirtilen bilgi ve malzemelerin biyoteknoloji ve tıbbi araştırma alanlarında değerli olacağına inanılmaktayım.

ACKNOWLEDGEMENTS

The preparation of this thesis would not be possible without those who have supported and inspired me through my master's study.

First of all, I would like to express my gratitude to my supervisor Asst. Prof. Havva Funda Yağcı Acar from Koç University for her guidance at all steps of my research and writing this thesis. Her support, motivation, enthusiasm and endless energy helped me during my research. I also appreciate her for her friendly attitude and advices about my private issues. Prof. Mehmet S. Somer and Prof. Alphan Sennaroğlu deserve special thanks as my thesis committee members and advisors.

I want to sincerely thank to every member of my family for their everlasting support, help and love during my whole life. My father (Ekrem Sevinç), mother (Semra Sevinç), elder sister (Tuğba Sakarkaya) and her husband (Umut Sakarkaya), and my little sister (Ayça Sevinç) motivated and encouraged me all the time and helped me to get over the hard times of my life and my research. In addition, I am deeply grateful to have such a precious fiance, İlker Onur Kaya, whose love, patience and support has never been ended since 2002.

I want to express thanks to my lab mates and colleagues. My graduated lab-mate Serdar Çelebi who achieved many implementations in the laboratory, shared many ideas and information about my research. I have learned a lot from him. He supported me at the initial stages of my research and my first experiment in the laboratory was accomplished by his help. I want to thank Sinan Öztürk for his instruction of instruments and experiments, and his patience to my endless questions. Recep Kaş also deserves gratitude due to his help and motivation through my research. I deeply appreciate Dr. Gökhan Çaylı because he never hesitated to share his deep knowledge and novel ideas with me and had always time for help whenever I needed during my research. I also would like to thank to my lab

partners Hande Öztürk, Ceren Yılmaz and Bilinç Barçın for their friendship and support. I am grateful to Selçuk Acar who supported me in the experimental part by preparing a critical material for my synthesis. I also thank him for his friendship and help outside of the laboratory. I would like to express my thanks to Feyza Selçuk, Hüseyin Çankaya and Can Özen from METU for their collaborations in my research, Prof. Mehmet Somer and Prof. Levent Demirel for their permission to use the instruments of their laboratories, Cevriye Koz for her assistance about everything in the inorganic research laboratory. I am also grateful to Muarrem Güler, the glass master, for his support for my reactions. Besides, I would like to thank Ali Baş, Burcu Uslu, Pınar Tatar and Merve Kocakuşakoğulları for their friendship, geniality inside and outside the department and motivation when I am in desperate mood.

Finally, I would like to acknowledge TÜBİTAK for financial support by providing scholarship throughout my master study.

TABLE OF CONTENTS

LIST OF TABLES

LIST OF FIGURES

NOMENCLATURE

QD	quantum dot
QY	quantum yield
STM	scanning tunneling microscope
DMSA	meso-2,3-dimercaptosuccinic acid
TGA	thioglycolic acid
3-MPA	3-mercaptopropionic acid
2-MPA	2-mercaptopropionic acid
TAA	thioacetamide
TOP	trioctylphosphine
TOPO	trioctylphosphineoxide
FWHM	full width at half maximum
DOS	density of states
LED	light emitting diode
UV	ultraviolet
IR	infrared
NIR	near infrared
NIRF	near infrared fluorescence
UV-Vis	ultraviolet-visible-near infrared
PL	photoluminescence
FTIR	fourier transform infrared
XRD	powder x-ray diffraction
-COOH	carboxylic acid group
-SH	thiol group
Eg	band gap energy

E_C	conduction band energy
E_v	valance band energy
E_{Ry}	Rydgerg energy
E_k	kinetic energy of carriers
E_{Coul}	coulomb energy
h	Planck's constant
r	average radius of quantum dots
d	average diameter of quantum dots
μ	reduced mass of the exciton
m^*_e	effective mass of electron
m^*_h	effective mass of hole
m_e	mass of electron
e	electron charge
ε	dielectric constant
ε_o	vacuum permittivity (or electric constant)
c	speed of light
ν	frequency of electromagnetic radiation
λ	wavelength of electromagnetic radiation
$I(\lambda)$	relative intensity of excitation light at wavelength λ
$A(\lambda)$	absorbance at the excitation wavelength λ
n	average refractive index of a solution
D	integrated area under the corrected emission spectrum
τ	fluorescence lifetime
pH	potential hydronium ion concentration
pKa	acid dissociation constant
nm	nanometer

Chapter 1

INTRODUCTION

"Nano-scale science and technology", shortly "nanotechnology", made production and characterization of materials with physical properties between atomic/molecular and bulk level possible. Sizes of these artificial materials are within the nanometer scale (equal to or less than 100 nm at least in one dimension). Nanotechnology is composed of research areas of physics, chemistry, material science, engineering and molecular biology which contribute to the fabrication, development and application of new nano-materials.

Nanotechnology was originated from a talk, "There's Plenty of Room at the Bottom", made by physicist Richard Feynman at an American Physical Society meeting at Caltech on December 29, 1959. He brought forward the possibility of manipulation of individual atoms and molecules of matter and importance of small-scale in this lecture. However, the definition of "nanotechnology" was first done by Norio Taniguchi in 1974. He defined nanotechnology as 'the processing, separation, consolidation, and deformation of materials by one atom or by one molecule'. In the early 1980s, the term got its current meaning and started with the development of cluster science and scanning tunneling microscope (STM).

The development of nanotechnology resulted in the discovery of novel nano-materials having physical and chemical properties significantly different from their bulk properties. Fullerenes[1], carbon nanotubes[2], metal and metal oxide nanoparticles and semiconductor quantum dots were examples of these. The common and noteworthy difference from the bulk property is that they have much higher surface to volume ratio or

surface area. This increases the chemical reactivity on the surface of these nano-materials. When size is reduced to nano, strength, electrical and thermal conductivity, optical output and elasticity are the examples of properties improved significantly. The behavior of charge carriers (electrons and holes) also change in this size scale meaning classical mechanics is not valid but principles of quantum mechanics should be considered to explain the changes in the properties of materials.

Development of bio-applicable quantum dots is the main purpose of the research covered in this M.S. thesis. Thus, quantum dots will be highlighted in this chapter. In the first section (1.1), quantum dots, their types, optical properties and electronic band structures will be summarized. Moreover, how the properties of these materials differ from their bulk properties will be mentioned and unique tunable band gap property by quantum confinement effect will be emphasized. Next section (1.2) is about the size and quantum yield determination methods and formulations. Sections 1.3 and 1.4 give a literature review for the synthesis and bio-applications of quantum dots, respectively. At the hearth of this research lies the "DMSA (meso-2,3-dimercaptosuccinic acid)", therefore, significance of DMSA will be discussed in the last section (1.5)

1.1 Quantum Dots (QDs)

Quantum dots are unique tiny semiconductors having crystal sizes usually between 1-10 nm. An average size quantum dot is around 25000 times smaller than one strand of human hair. Semiconductor dots are composed of elements from the II-VI (i.e. CdS, CdTe, and ZnSe), III-V (i.e. GaAs, InP) or IV-VI (i.e. PbS, SnTe) groups of the periodic table. They behave differently than the bulk semiconductors of these elements. Quantum dots are unique electromagnetic emitters with a tunable band gap as a result of the quantum confinement occurring in the nanoscale semiconductors when sizes are below the exciton Bohr radius [3].These concepts will further be discussed in the following sections in detail.

1.1.1 Electronic Band Structure and Quantum Confinement Effect

The electronic band structure of a bulk semiconductor is composed of continuous energy levels and a band gap (forbidden energy level) between these levels, as represented in Figure 1.1(A). Energy states above the band gap is called the conduction band which is unoccupied by electrons. The energy states lying below the band gap is called the valance band, fully occupied by the valance electrons. Each bulk semiconductor has its intrinsic band gap energy (E_g) ranging from a fraction of an eV to a few eV. The band gap energy is the energy difference between minimum level of conduction band (E_c) and maximum level of valance band (E_v) (Figure 1.1(A)).

When sufficient energy (greater than the band gap energy) in the form of heat, voltage or photon is applied to semiconductors, an electron (negative charge carrier) in the valance band can be excited to the conduction band. The excited electron leaves an empty electronic state or hole (positive charge carrier) behind and the electron-hole pair, which is called *exciton*, forms. The distance between the exciton pair is called *Exciton Bohr Radius* (Figure 1.1 (B)).

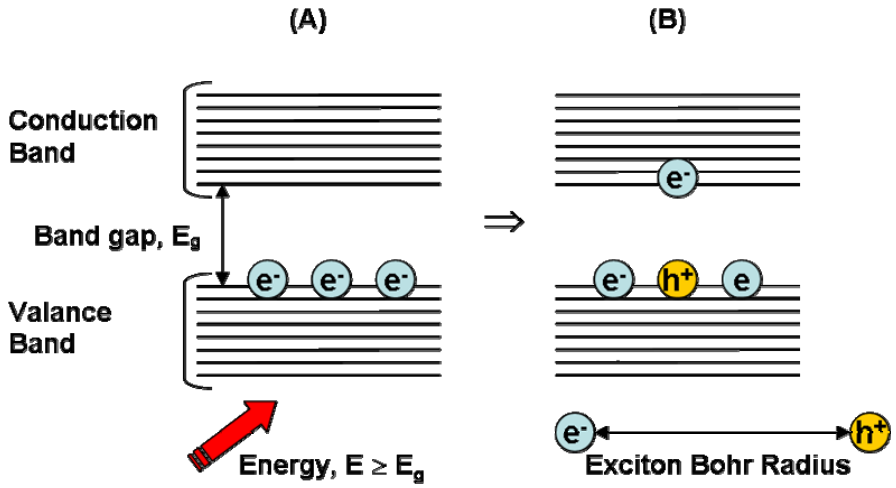

Figure 1.1 A simplified electronic band structure of bulk semiconductor (A) and exciton (B)

When the size is sufficiently small, the (bulk) exciton Bohr radius becomes comparable to, or even bigger than the crystal dimensions. However, due to the potential barrier at the surface of the crystal, the exciton can not form beyond the edge of the crystal. As a result, the exciton will have to be squeezed to fit into the crystal increasing their kinetic energy in this confined area. This situation is called as *quantum confinement*, and as a consequence of this confinement, the continuity of the bands will be lost and discrete energy levels appear. Therefore, Exciton Bohr Radius is the limit for physical dimension of a semiconductor to have continuous energy levels. Moreover, the band gap of quantum dots turns out to be greater than that of the bulk crystals. If this confinement is in three dimensions, these tiny semiconductor crystals are called as *'quantum dots'*. Further shrinkage of QDs causes more confined charge carriers leading to a greater separation between the individual energy levels and a larger band gap. The quantum confinement effect on energy levels and band gap can be clearly seen in Figure 1.2.

QDs fluoresce as a result of the recombination of excited electrons with holes. Their optical properties are also affected by the bad gap change as a consequence of the quantum confinement. As the size of QDs gets smaller, light absorption and emission occurs at a shorter wavelength as the band gap increases. In Figure 1.2, the color of emitted light is represented on the dots with size change. Detailed discussion about this unique, size tunable optical property of QDs will be in the next section.

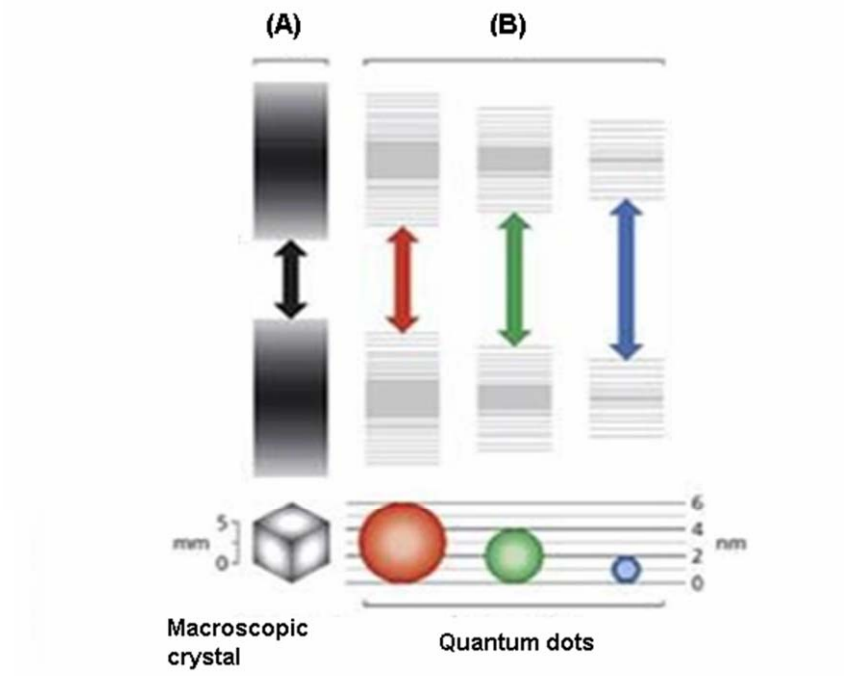

Figure 1.2 Quantum confinement effect on energy levels and band gap of quantum dots: Bulk semiconductor (A) and Quantum dots (colors represent the emitted light) (B) (www.tudelft.nl/live/pagina.jsp)

Dimensions of quantum confinement determine the type of the semiconductor nanostructure. In bulk semiconductors, electrons are free to move in all three directions. When the solid is extended in two directions but its thickness along the third dimension is only a few nm, the electrons' movement is restricted along the third direction. Then, this two-dimensional system with one dimensional quantum confinement is called *quantum wells*. If the confinement appears to be in two dimensions, these one dimensional structures are called *quantum wires*. Finally, three dimensional confinement leads to *quantum dots* as mentioned before. QDs are zero-dimensional systems. Confinement of electrons affects the density of states (DOS) of these solids as represented in Figure 1.3. Starting from

continuous in the bulk structure, density of states become discrete as the dimension of confinement is raised.

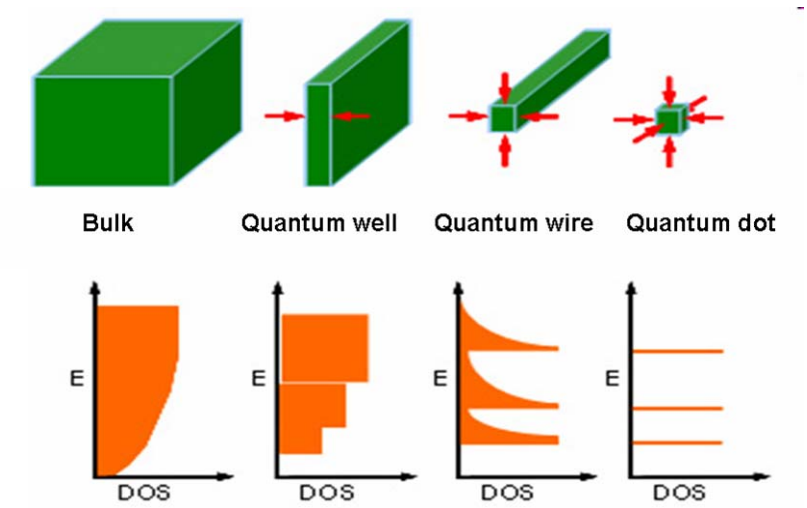

Figure 1.3 Dimensional quantum confinement and its effect on density of states (www.stkc.go.th/stportalDocument/1204088345.html)

1.1.2 Size Tunable Optical Properties

Quantum dots are fluorescent nanocrystals and they have unique size dependent tunable band gap as discussed in the previous section. When electromagnetic radiation having a specific energy is applied to quantum dots, an electron staying in the valance band (ground state) is excited to higher energy levels in the conduction band leaving a hole behind (Figure 1.4). This process is called the absorption of light. Light can be absorbed by the quantum dot only when its energy is equal to or higher than the band gap energy, Eg. Since the band gap of a quantum dot is size dependent, the absorption energy also depends on size.

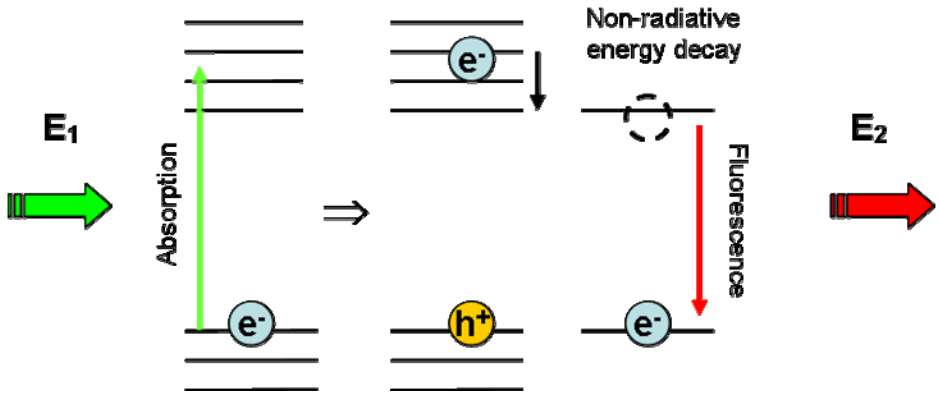

Figure 1.4 A basic scheme of the fluorescence mechanism of QDs

The excited electron has a tendency to relax back to its original position, ground state. Therefore, recombination of the electron with the hole takes place quickly. During the recombination, either a non-radiative or a radiative decay occurs (Figure 1.4). Radiative decay causing an energy loss by the emission of photons is called *fluorescence of light*. Energy of the emitted photon depends on the band gap, consequently on the size of the quantum dot. Non-radiative decay occurs during the transition of an electron through the vibrational modes of the conduction band or at the trap sites yielding phonon scattering. However, this non-radiative energy loss is very small in quantum dots because phonon scattering rates significantly decrease with increasing energy-level separation[4, 5].

Absorption spectra of quantum dots are composed of series of overlapping peaks of the incident electromagnetic radiation absorbed over a range of wavelengths. The wavelength at which discontinuity starts is called *absorption edge (onset)* and it also referred as the starting point of the exciton absorption in the spectrum. It depends on the size (band gap) of the particles and the first correct interpretation of this size dependent absorption by quantum confinement was done by L. Brus [6]. In Figure 1.5, it is shown that smaller quantum dots have an absorption edge that is shifted to shorter wavelengths with respect to larger quantum dots.

Fluorescence spectra show the intensity of emitted light resulting from the recombination of photo-excited electron-hole pair. The peak emission wavelength is not affected from the excitation wavelength but determined by the size of quantum dots because the fluorescence spectra only shows the transitions from the lowest excited state to the ground state which is equal to the band gap of the nanoparticle[7]. That's why emission wavelength shifts towards longer wavelengths in the fluorescence spectra as the band gap decreases (or size increases) (Figure 1.5). The spectrum also reflects the size distribution of quantum dots. It is a Gaussian shaped curve and the bandwidth of this curve, called *Full Width at Half Maximum* (FWHM), gives information about the size distribution of quantum dots. Smaller the FWHM is, narrower the size distribution.

When absorption and emission spectrum of quantum dots are stacked as illustrated in Figure 1.5, a clear shift is observed between the lowest energy peak in the absorption spectrum and the corresponding emission peak. Here, the energy absorbed is greater than the energy of fluorescence which is called the *''Stokes shift''*. This shift appears due to non-radiative relaxations of electron or other energy losses like collisions with other molecules to lose vibrational energy until the particle reaches the lowest vibrational state of the excited electronic state.

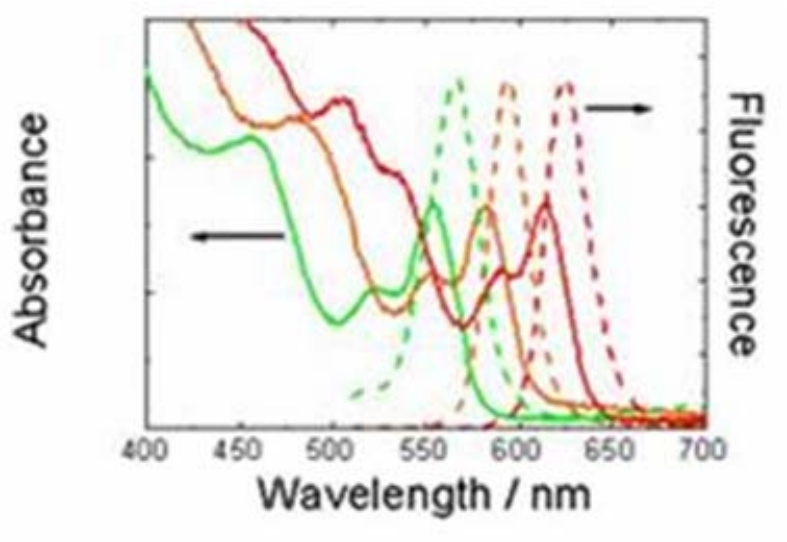

Figure 1.5 Representation of absorbance and fluorescence spectra of CdTe QDs. Color of the graphic represents the emission color of the QDs. (www.wiseman-group.mcgill.ca/heyes.php)

1.1.3 Structures of QDs

QDs have been synthesized in the form of an inorganic core (semiconductor crystal) surrounded by an organic surfactant (ligand) until the last few years (see Figure 1.6(A)). Recently, core/shell heterostructures have become essential in order to improve the quality of QDs. The shell reduces non-radiative recombination and the effects of surface defects resulting in a brighter luminescence. This core/shell structure is composed of an inorganic core surrounded by another inorganic semiconductor layer and a surfactant at the outer-most section (see Figure 1.6(B)). The organic surfactant has a functional group such as thiol, amine, nitrile, phosphine or phosphine oxide and can be hydrophilic or hydrophobic. Through the bonding of appropriate molecules to the surface, quantum dots can be dispersed in solvents.

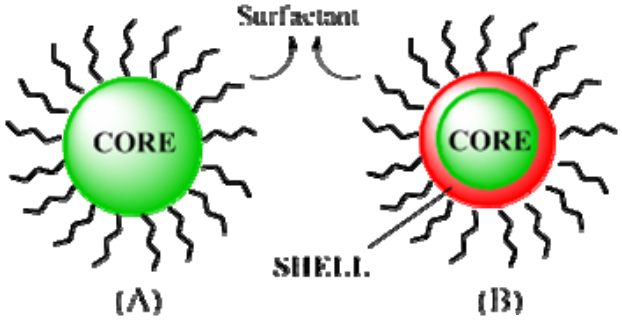

Figure 1.6 Schematic of a core (A) and a core/shell (B) quantum dot structure

This core/shell heterostructures are also separated into two groups: Type-I and Type-II. In Type-I quantum dots (CdSe/CdS[8, 9], CdSe/ZnS[10] and CdTe/CdS[11]) core is covered by a larger band gap material. Here, the band offsets are arranged in such a way that the conduction band of the shell is at a higher energy level than that of the core and the valence band of the shell is at a lower energy than that of the core (Figure 1.7). Consequently, both electrons and holes are confined in cores and the radiative exciton recombination occurs here. A type-II quantum dot, on the contrary, has both the valence and conduction bands of the core at the lower (or higher) energy level than the shell. As a result, charge carriers are separated in a way that one carrier is mostly confined in the core, while the other is mostly confined in the shell (Figure 1.7). Then, the radiative recombination takes place across the core-shell interface. CdTe/CdSe[12] and CdSe/ZnTe[12] are examples of type-II quantum dots. Type-II quantum dots are effective for Near Infra-Red (NIR) emission. In addition to these core/shell structures, studies on multilayered quantum dots have been started as well. CdSe/CdTe/ZnTe [13], CdSe/CdS/ZnS and CdSe/ZnSe/ZnS[14] core/shell/shell quantum dots are examples of multilayered dots.

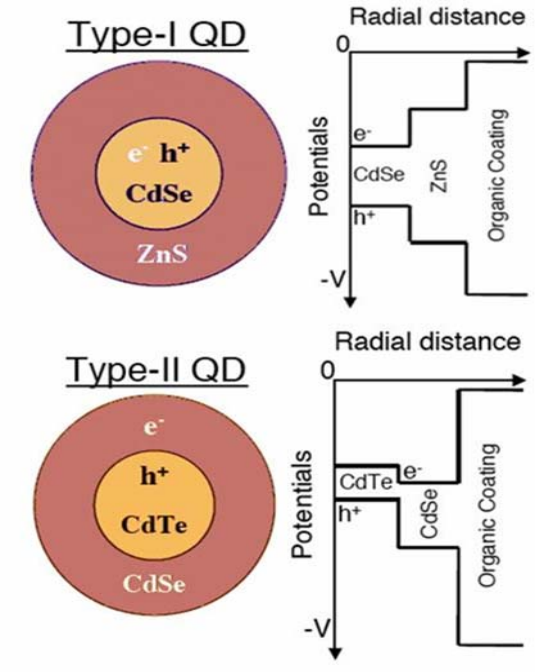

Figure 1.7 Representation of band structures for Type-I and Type-II Quantum Dots. (nanocluster.mit.edu/research.php)

1.2 Characterization of QDs

1.2.1 Brus Equation and Particle Size Calculation

The size dependence of the electronic properties of small semiconductor crystallites was first studied by L. Brus in 1984 [15]. In his work, the excited electronic states of these particles were modeled and an approximate formula for the lowest excited electronic state energy of these nano spheres was established by a modification of the Schrödinger's equation as [15, 16]:

$$E_g(dot) = E_g(bulk) + \frac{h^2}{8r^2}\left[\frac{1}{m^*_e} + \frac{1}{m^*_h}\right] - 1.8\frac{e^2}{4\pi\varepsilon\varepsilon_0 r} \tag{1.1}$$

This equation is an expression of size dependent band gap energy of quantum dots and is composed of three terms which are needed to be discussed briefly: The first term is the bulk (infinite crystal) band gap energy of the semiconductor, E_g(bulk). The second one is the kinetic energy of carriers or energy of localization. This term can also be defined as the quantum confinement energy of carriers, and is a combination of particle in a box model with an effective mass approximation. This expression is adapted to quantum dots from the zero point energy of the potential well, or in other words, the energy of the state of a potential box with the lowest energy. This can be written as:

$$E_k = \frac{h^2}{8\mu r^2} \tag{1.2}$$

where h is Planck's constant, r is the average radius of the particles and μ is the reduced mass of the exciton and is given as $\mu^{-1} = m^{*}{}_{e}^{-1} + m^{*}{}_{h}^{-1}$. Here, reduced mass is assigned to the exciton because an exciton is considered to behave as a single particle moving with a center of mass motion in theory. Moreover, this reduced mass is defined by the effective masses of the electron and hole, represented as m^{*}_{e} and m^{*}_{h}, respectively, because they cannot be treated as 'free' electrons in metals due to their interactions with semiconductor lattice. This treatment is called the *effective mass approximation*. The last term (E_{Coul}) is the screened Coulomb energy (interaction) which represents the attraction between the electron and the hole. Screening strength depends on the dielectric constant, ε, of the semiconductor. Coulomb term is given as:

$$E_{Coul} = -1.8\frac{e^2}{4\pi\varepsilon\varepsilon_0 r} \tag{1.3}$$

In Equation 1.1, the size dependence is emphasized in two terms: the confinement energy, which is proportional to $1/r^2$, and the Coulomb attraction, which is proportional

to $1/r$. Due to the $1/r^2$ factor, confinement effect becomes dominant in determining the band gap energy of small size quantum dots.

Equation 1.1 is also a basic approximation neglecting additional effects such as crystal anisotropy and spin-orbit coupling [17]. Moreover, the spatial correlation between the charge carriers can be significant when the dielectric constant is small. Therefore, a fourth term, Rydgerg energy (E_{Ry}), which is also size independent, appears to be another term to be added for band gap energy calculations of these particles[18]. Rydgerg energy is given by:

$$E_{Ry} = \frac{2e^4\pi^2}{\varepsilon^2 h^2}\left[\frac{1}{m^*_e} + \frac{1}{m^*_h}\right]^{-1} \tag{1.4}$$

Since $E_g(dot)$ is equal to the minimum energy of absorbed light required to create an exciton, an average size can be calculated for synthesized quantum dots by using Brus equation (Eqn. 1.1) and absorption edge from the absorption spectrum. Therefore, $E_g(dot)$ can be written in the form of Planck equation as:

$$E_g(dot) = h\nu_{edge} = h\frac{c}{\lambda_{edge}} \tag{1.5}$$

where c is the speed of light, ν_{edge} and λ_{edge} are the frequency and wavelength corresponding to the absorption edge of quantum dots. Combination of Eqs. (1.1) and (1.5) gives the final form of the equation for particle size calculation:

$$h\frac{c}{\lambda_{edge}} = E_g(bulk) + \frac{h^2}{8r^2}\left[\frac{1}{m^*_e} + \frac{1}{m^*_h}\right] - 1.8\frac{e^2}{4\pi\varepsilon\varepsilon_0 r} \tag{1.6}$$

Detailed calculations with the appropriate parameters for the quantum dots prepared in this research will be given in Appendix.

1.2.2 Quantum Yield (QY) Calculation

Quantum yield is the ratio of the number of emitted photons to the number of absorbed photons. Quantum yield indicates the optical quality of quantum dots. The higher the quantum yield, the greater the number of emitted photons, in other words, the greater is the efficiency. As discussed in section 1.1.2, some of the absorbed energy is lost by non-radiative decays either in the conduction band or in trap sites. Therefore, it is not possible to have 100% QY.

Quantum yield of quantum dots is estimated in comparison with reference materials (organic fluorophores) such as Rhodamine B and Rhodamine 6G. The calculation is done according to the following equation[19]:

$$Q_x = Q_r \left(\frac{A_r(\lambda_r)}{A_x(\lambda_x)} \right) \left(\frac{I(\lambda_r)}{I(\lambda_x)} \right) \left(\frac{{n_x}^2}{{n_r}^2} \right) \left(\frac{D_x}{D_r} \right) \tag{1.7}$$

where Q is the QY, $I(\lambda)$ is the relative intensity of excitation light at wavelength λ, $A(\lambda)$ is the absorbance at the excitation wavelength λ, n is the average refractive index of the solution, D is the integrated area under the corrected emission spectrum. Here, r and x denotes reference and quantum dot sample.

If the reference material and quantum dot solutions are in the same solvent and excited at the same wavelength, both $\left(\frac{{n_x}^2}{{n_r}^2} \right)$ and $\left(\frac{I(\lambda_r)}{I(\lambda_x)} \right)$ terms become 1.0 and Eqn. 1.8 has its simpler form as:

$$Q_x = Q_r \left(\frac{D_x / A_x(\lambda x)}{D_r / A_r(\lambda r)} \right) \tag{1.8}$$

1.3 Synthesis of Colloidal QDs

Colloidal quantum dots are chemically synthesized by wet chemistry and grown in the reaction solution. The fabrication of colloidal quantum dots includes a reaction flask as a reactor and a liquid mixture of precursors required for the nucleation and growth. The energy required for the growth is supplied by the liquid in the reactor, either by thermal collisions of precursors or by a chemical reaction between the solvent and the precursors, or both [20].

Quantum dots have been mostly synthesized in high boiling point organic solvents such as trioctylphosphine (TOP) or trioctylphosphineoxide (TOPO) or a mixture of TOP and TOPO [8, 21-25] producing hydrophobic particles with high quantum yield. However, this hydrophobic nature prevented these QDs to be applicable in biological applications. Therefore, suspension in water was achieved via ligand exchange which, on the other hand, decreased the quantum yield and colloidal stability of these materials [21-25]. To eliminate these drawbacks, direct aqueous synthesis by employing hydrophilic thiols as stabilizing agents was preferred. Thiols passivate surface dangling bonds, and contribute to the stability, solubility and surface functionality of the nanoparticles. Thioglycolic acid (TGA) and 3-mercaptopropionic acid (3-MPA) are the most widely used thiolated ligands in aq. QD synthesis [26-28].

In recent years, aqueous synthesis methods of QDs have been dramatically improved by adaptation of hydrothermal synthesis method using an autoclave with higher reaction temperatures[29-31] and temperature controllable microwave reactor method [32]. Moreover, core/shell QDs such as CdSe/CdS[9, 33] and CdTe/CdS[11, 34-37] has been very popular in obtaining effectively passivated core surface and improve optical properties of the core QDs. In these syntheses, CdS shell formation was achieved by using Na_2S[9] as a direct source of sulfur or by the decomposition of thioacetamide[11, 33] and thiourea[37] providing a slow release of sulfur to the reaction medium. According to the studies on the

direct synthesis of CdTe/CdS core/shell structures, QY of the core QD improves significantly with the formation of the shell. Post-synthesis illumination techniques are also applied to form a CdS shell by the photo-induced decomposition of organic thiolated surfactant releasing sulfur ions (i.e. TGA)[34]. Therefore, with an appropriate ligand and conditions, it should possible to prepare CdS QDs through the decomposition of the thiolated organic material. Such an approach would be much easier and more practical compared to the previous methods[20, 38, 39].

1.4 Bio-applications of QDs

Quantum dots are a novel class of inorganic fluorophores with their unique optical properties. They are rapidly being applied to the existing and emerging technologies in many areas. Some examples for the electronic and optical applications of quantum dots are lasers, solar cells, light emitting diodes (LEDs), sensors [40-42]. However, current research that will be discussed in this thesis mostly concerns about the biological applications of quantum dots and the most highlighted topics are gene technology, cell tracking, tumor biology investigation, diagnostics, biomedical labeling and *in vivo* imaging[43-46].

Quantum dots are preferred to organic fluorophores (dyes) in bio-applications because their optical properties are more advantageous than the conventional dyes: In addition to the size tunable emission wavelength discussed in the previous chapters, different-sized dots can be excited simultaneously by a single light source, meaning, multiple emission colors can be achieved at once by using the same excitation wavelength. Quantum dots also have many orders of magnitude longer lifetime than conventional organic fluorophores, allowing detection at a larger timescale. Narrow and symmetric emission spectra is also advantages when especially multicolored arrays are required [47]. In addition, quantum dots have large emission range form the ultraviolet (UV) to the infrared (IR) (400-1350 nm) [48]. Near infrared (NIR) quantum dots can offer deep tissue imaging in living

subjects due to the low absorbance and scattering of the skin in the NIR region (700-900 nm). Moreover, no good organic fluorophores exist in the NIR range [49].

These significant advantages over organic dyes, fluorescent proteins and lanthanide probes made quantum dots preferential in ultrasensitive, multicolor and multiplexed imaging applications in molecular biotechnology and bioengineering [47]. Besides, they are more advantageous in imaging techniques (i.e. two-photon or time-gated microscopy) and they are good candidates as near infrared fluorescence (NIRF) probes [48, 49].

1.5 Why DMSA?

In this work, a novel material, meso-2, 3-dimercaptosuccinic acid (DMSA), is chosen as the stabilizing ligand for the synthesis of aqueous CdS and CdTe/CdS core/shell QDs. There are several significant reasons for this choice. DMSA was previously used as a biocompatible surfactant to thiolate iron oxide nanoparticles successfully [50-53]. DMSA is bio-compatible and a good metal chelating agent [54] and therefore it is used to treat arsenic and mercury poisoning in human body [55]. Chemical structure of DMSA consists of two thiol (pK_{S1}= 9.65 and pK_{S2}= 12.05) and two carboxylic acid groups (pK_{C1}= 2.71 and pK_{C2}= 3.43) [54] (Figure 1.8). Thus, it is hydrophilic and can provide electrostatic stabilization in water. Furthermore, DMSA is expected to provide good passivation of surface by the thiols and conjugate with biomolecules via -COOH groups.

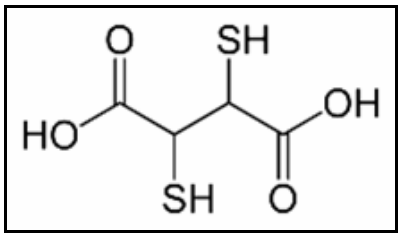

Figure 1.8 Meso-2,3-dimercaptosuccinic acid (DMSA) structure

1.6 Objective of This Research

In the research area of medicine, there is a growing need for highly luminescent, stable, colloidal bio-compatible aqueous quantum dots. Actually, quantum dots are preferred to organic fluorophores due to their relatively small sizes, narrow FWHM and high stability against photobleaching. Especially for diagnostics and bio-imaging of deep living tissue, quantum dots are expected to fluoresce in the NIR region in order to eliminate the absorption and scattering effects of the tissue. Moreover, there are many studies on preparation techniques and structures of quantum dots to improve their optical efficiency. Recently, the construction of core/shell nanoparticles emerged as an effective method to remove defects at the particle surface and the interface, reducing the non-radiative energy transitions. Here, selection of the appropriate stabilizer is also very crucial because its properties should satisfy the needs of a biological use, for instance, it should be non-toxic and have functional groups for conjugation with biomolecules and it should provide a good passivation and stability to QDs in water.

Being conscious of these needs, it is aimed at developing highly luminescent, colloidal aqueous quantum dots which are applicable to biological systems. In order to achieve such goal DMSA was chosen as the stabilizer (surfactant), which has not been used in quantum dot synthesis before. DMSA was a perfect candidate when the biological issues concerned since it is non-toxic, bio-compatible and used as a chelating agent of hard metals in human body. Moreover, having two thiols and carboxylic acid groups in its structure, it promises good passivation by thiols and water solubility by carboxylic acid groups. In our research group, there is a substantial experience with CdS QDs, therefore as the first step, synthesis of DMSA capped CdS quantum dots were planned. DMSA was expected to provide better passivation and bio-compatibility to these nanoparticles. As a second step; development of CdTe/CdS core/shell quantum dots by the help of DMSA was aimed. Here, the reason for choosing CdTe as the core material is the fact that CdTe quantum dots are preferred for

bio-applications due to its emission spectra close to the NIR region. CdS shell growth was aimed to achieve brighter emission of these quantum dots.

Chapter 2

EXPERIMENTAL

2.1 Materials

Cadmium acetate dihydrate ($Cd(CH_3COO)_2.2H_2O$, 98%), 2-mercaptopropionic acid (2-MPA, $C_3H_6O_2S$, ≥96%) and thioacetamide (TAA, CH_3CSNH_2, ≥99%) were purchased from Merck. Meso-2,3-dimercaptosuccinic acid (DMSA, $C_4H_6O_4S_2$, ≥97%) and Rhodamine (B and 6G) were purchased from Fluka. Milli-Q water (Millipore) was used as the solvent and all of the chemicals were used as received without further purification.

2.2 Experimental Section

2.2.1 Synthesis of DMSA capped CdS QDs

Cadmium acetate (53.3 mg, $Cd(CH_3COO)_2.2H_2O$) was dissolved in 80 mL water in a three-necked round-bottom flask. Twenty milliliters of DMSA solution prepared by sonication of the required amount of DMSA in water at 70ºC was added to the Cd-solution at room temperature, and then the pH was adjusted to 7.5 with 1M NaOH under N_2 flow. This Cd/DMSA solution was deoxygenated for 15 min with nitrogen, and then the solution was heated to 70ºC. The amount of DMSA required was expressed as SH/Cd mol ratio. SH/Cd ratio between 1.5-7 was studied.. Each DMSA molecule contains two SH. Duration of the reactions depends on the amount of DMSA and shortens as the amount increases.

2.2.2 Synthesis of Na_2Te

The synthesis of Na_2Te was adopted from an earlier report [56]. Stoichiometric amounts of elemental Na and Te were placed in a silica schlenk tube under inert atmosphere in a glove box (O_2 and H_2O below 1 ppm).

$$2Na + Te \rightarrow Na_2Te \quad (2.1)$$

The tube connected to the vacuum line (Figure 2.1(A)) where the system was vacuumed above 10^{-3} mbar pressure in order to remove oxygen. Then, the reaction tube was placed into a liquid nitrogen bath (Figure 2.1(B)) which was a cold temperature trap to be used at the next step. Liquid nitrogen bath improves the vacuum performance, as well.

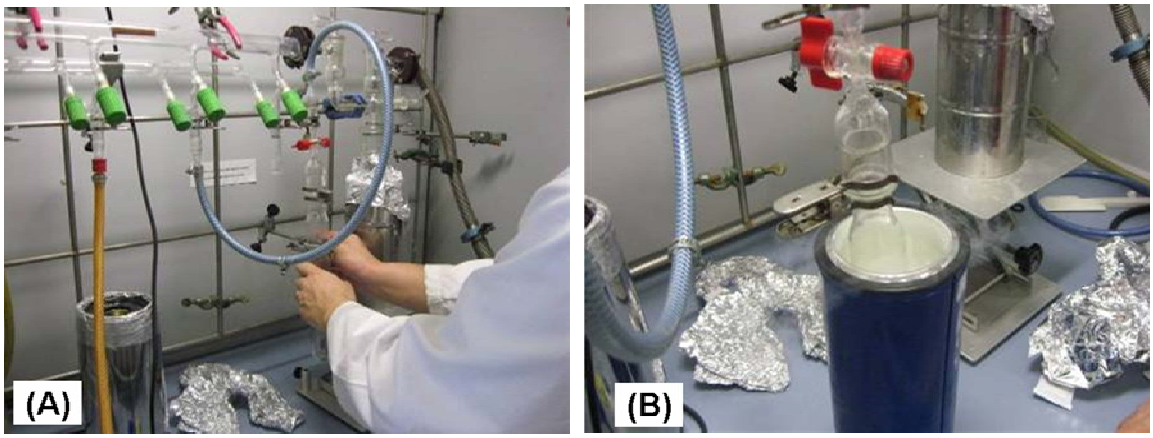

Figure 2.1 Connection of Na and Te mixture to the vacuum line (A), Liquid nitrogen bath (B)

Next, the vacuum line and the reaction tube were purged with constant ammonia (NH_3) gas flow. The NH_3 flow is condensed at the cold temperature trap since the liquid NH_3 acts as the solvent for Na_2Te synthesis. The formation of dark blue color was observed at -196 ºC (liquid N_2) (Figure 2.2(A)). After sufficient liquid NH_3 was obtained, the reaction tube

was placed in ca. - 40ºC liquid glycerol bath (Figure 2.2(B)) in order to achieve a slow reaction kinetics and a slow vaporization of NH_3 (B.P. of NH_3 = -33.3ºC). In addition, the tube was connected to the Hg manometer that acts as a pressure relief for NH_3 gas.

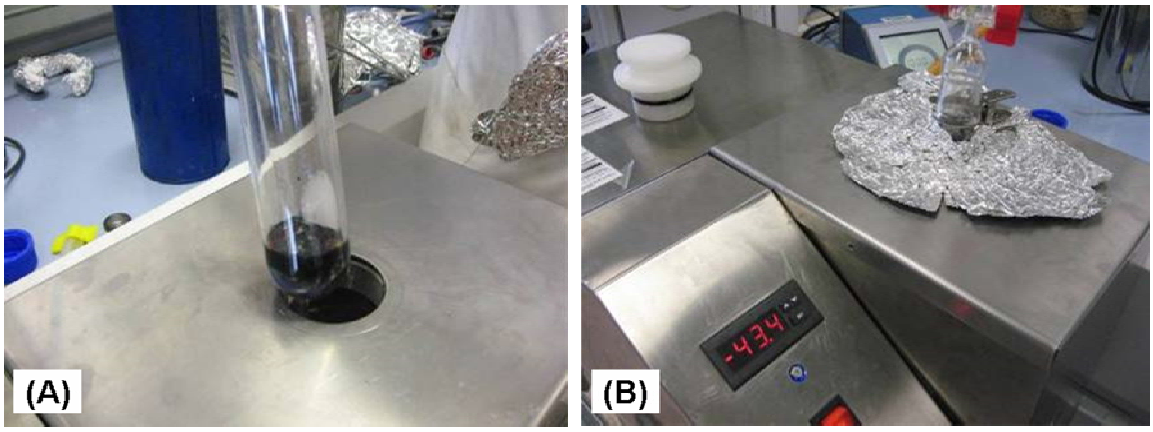

Figure 2.2 Dark blue color of condensed NH_3 (A), Liquid glycerol bath (B)

Evaporation of the NH_3 gas was continued very slowly for 36 hours. The color change on the walls of the tube from dark blue (liquid NH_3) to white (Na_2Te powder) proved the completion of the formation of Na_2Te reaction. Na_2Te was stored in a glove-box because it is a highly air-sensitive material.

2.2.3 Synthesis of 2-MPA capped CdTe QDs

A typical method would be as follows: Cadmium acetate (213.2 mg, $Cd(CH_3COO)_2.2H_2O$) and 2MPA were dissolved in 160 mL water in a four-necked round bottom flask fitted with a reflux condenser . The pH was adjusted to 9 with 1M NaOH under N_2 flow. After 30 min. of nitrogen purge, Na_2Te was weighed in the glow box (O_2 and H_2O below 1 ppm). Na_2Te was put in a perfectly sealed round bottom flask and 20 mL of oxygen free water was transferred into this flask through a stainless steel tubing from

another round-bottomed flask (Figure 2.3(A)). After dissolving all the Na_2Te powder under N_2 flow, 20 mL of purple Na_2Te solution was transferred into Cd-2MPA solution (Figure 2.3(B)). The solution temperature was immediately raised to 90ºC (Figure 2.3(C)).

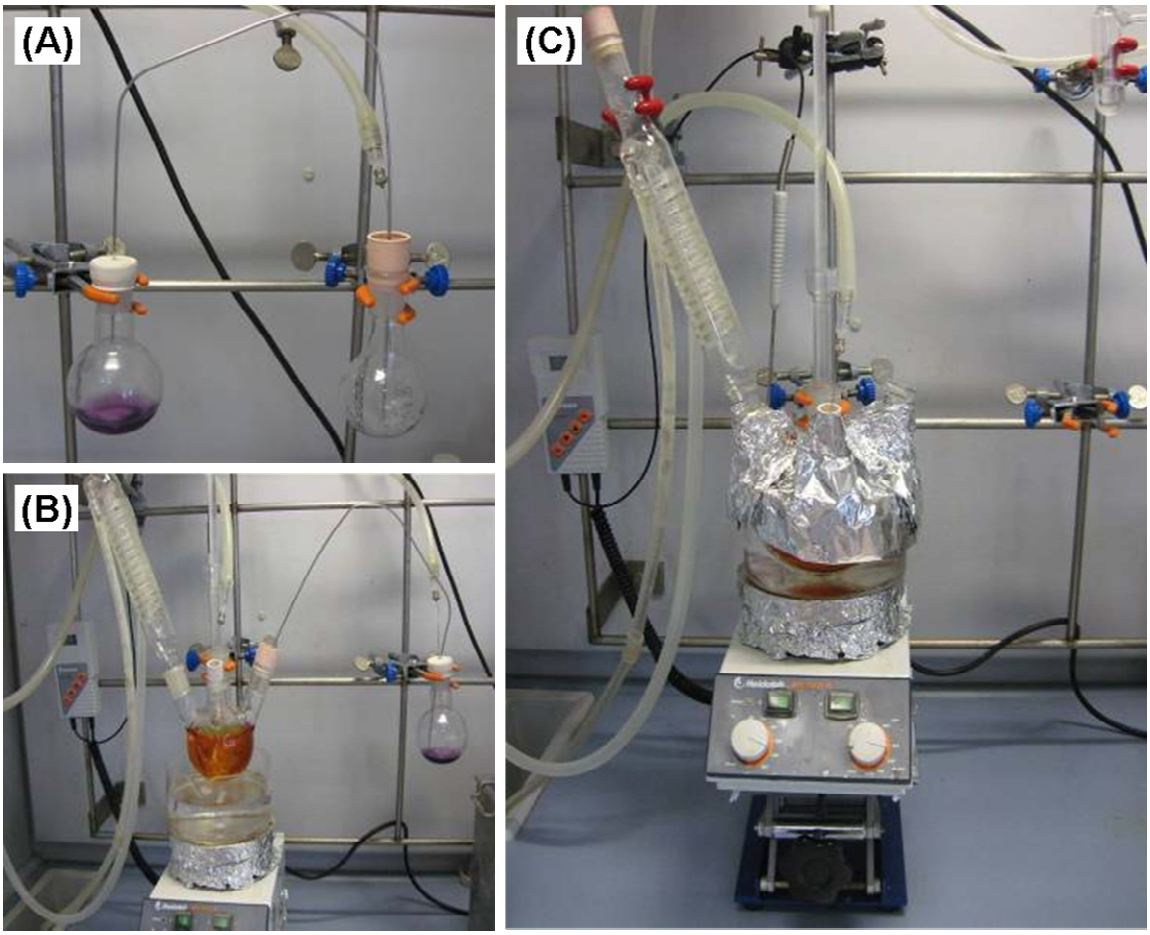

Figure 2.3 Transfer of oxygen free water to Na_2Te powder (A), Transfer of purple Na_2Te solution to Cd-2MPA complex solution and initial formation of orange CdTe solution (B), CdTe QD formation at 90ºC in silicon oil (C)

Duration of the reactions varied by the reaction conditions, i.e. pH and SH/Cd ratio. The molar ratio of Cd:Te:SH was 1:0.38:2.4. Different pH values (7.5 and 11.0) and SH/Cd ratios (1.5 and 5.0) were also studied to observe their effects on the particle properties. Samples were taken out at different time intervals to follow the particle growth and change in the particle properties. Samples were stored in a refrigerator.

2.2.4 Synthesis of CdTe/CdS core/shell QDs by the decomposition of DMSA

Twenty milliliters of aq. DMSA solution at various concentrations was added to the reaction of CdTe-2MPA at the fourth hour of the reaction described in 2.2.3. SH (from DMSA)/Cd (initial amount from CdTe synthesis) molar ratios of 1.0, 0.7 and 0.5 were studied. The QD concentration was kept constant referring to Cd^{2+} concentration. The particle size and QY was followed by taking out aliquots at regular intervals during the reflux.

Additionally, CdTe/CdS core/shell nanoparticles were prepared through thermal decomposition of thioacetamide by the same procedure at Cd^{2+}:Te^{2-}:SH(2-MPA)= 1.0:0.38: 2.4, molar ratio of SH(TAA)/Cd(initial) = 0.7 and initial pH of 9.0 .

2.3 Characterization

Ultraviolet-Visible-Near Infrared (UV-Vis) and Photoluminescence (PL) spectra were recorded with a Schimadzu UV-Vis-NIR spectrophotometer model 3101 PC and Horiba Jobin Yvon-Fluoromax 3 spectrofluorometer, respectively. All optical measurements were performed at room temperature under ambient conditions. PL spectra of CdS QDs were recorded in the range of 365 nm to 850 nm at a 0.5 nm interval at the excitation wavelength of 355 nm. A 370 nm filter was used for these measurements. For CdTe and CdTe/CdS QDs, PL measurements were done in the range of 410 nm to 800 nm at a 0.5 nm interval.

The excitation wavelength was 400 nm and emission filter had a cut-off at 450 nm. PL spectra were all calibrated with respect to absorption values at the excitation wavelength. Quantum yields were estimated according to the procedure of [19] by diluting the samples to three different concentrations having max 0.1 absorbance at the excitation wavelength of 355 nm and 400 nm for CdS and CdTe (CdTe/CdS) QDs, respectively. Rhodamine B (31% QY in water) was used for CdS and Rhodamine 6G (95% QY in ethanol) was used for CdTe (CdTe/CdS) as references. Brus Equation [15] was used to calculate the sizes of the CdS-DMSA and CdTe-2MPA nanoparticles. Samples for further characterization were prepared by multiple washing of QDs with water through 3K ultra-centrifugal filters at 3800 rpm in order to remove excess organic materials or inorganic ions from solutions. Fourier Transform Infrared (FTIR) spectra were obtained by Jasco FT-IR-600 spectrometer using KBr pallet of the dried samples. Samples were dried after washing in a Labconco freeze-drier unit. Powder x-ray diffraction (XRD) analysis was performed using a HUBER G670 diffractometer equipped with a germanium monochromatized CuKα radiation (λ=1.5406Å). Fluorescence lifetime measurements were conducted using Model C-71 Time Master time resolved fluorescence spectrometer from Photon Technology International (New Jersey, USA). A nanosecond flash lamp filled with nitrogen gas was used to excite samples at 355 and 400 nm. Data were collected from quadruplicate samples.

Chapter 3

RESULTS AND DISCUSSION

3.1 CdS-DMSA Results

3.1.1 Synthesis of DMSA capped CdS QDs via DMSA decomposition

In a typical synthesis, CdS nanocrystals have been prepared by using Na_2S as a sulfur source[20, 38, 39]. A CdS shell can be formed around CdTe nanoparticles by the decomposition of thioacetamide and thiourea [11, 34, 37]. Formation of a thin CdS layer around CdTe has been reported for thioglycolic acid (TGA) capped CdTe as a result of TGA decomposition [34]previously. Therefore, DMSA, having two thiol groups and being biocompatible, is predicted to be a good sulfur source for the synthesis of CdS nanocrystals by thermal decomposition as well as an efficient capping agent to prepare stable non-toxic CdS QDs.

The formation of CdS nanocrystals are confirmed by XRD. Figure 3.1 shows the XRD pattern of CdS nanocrystals which suits to the cubic zinc blende structure. The peaks are broad as it is expected in nanocrystals. Moreover, this broadness resulted in an overlapping of the peaks at 42º and 52º which is seen as a single peak in the diagram because of the extremely small size of the crystals.

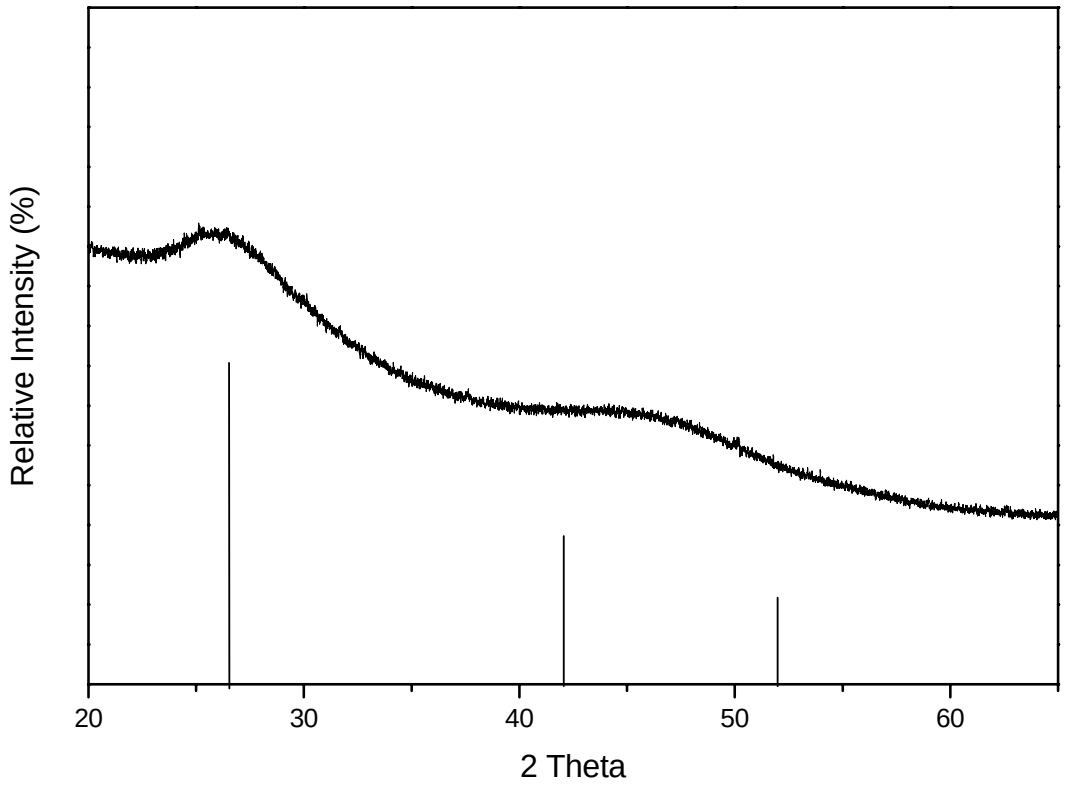

Figure 3.1 Powder X-ray diffractogram of ES24G.

FTIR spectra have provided us information about the thiol and carboxylic acid groups during the QD formation. As it is shown in figure 3.2, DMSA has the characteristic peaks of S-H band at 2564.8 cm^{-1} and C=O stretching band corresponding to carboxylic acid at 1720.4 cm^{-1}. Spectra of Cd-DMSA complex and CdS-DMSA show antisymmetric and symmetric stretching modes of carboxylate at around 1580 cm^{-1} and 1388 cm^{-1}. Moreover, S-H band broadens for the Cd-DMSA complex and finally disappears as CdS nanocrystals form with the sulfur release from DMSA. This situation can be explained in two ways; either DMSA is decomposed to give all of its sulfurs and stabilization is supplied by carboxylates or only one of its sulfurs is released to form CdS and the remaining thiolate is

used to passivate the CdS surface which is more probable when the stability and luminescence properties of the particles are considered.

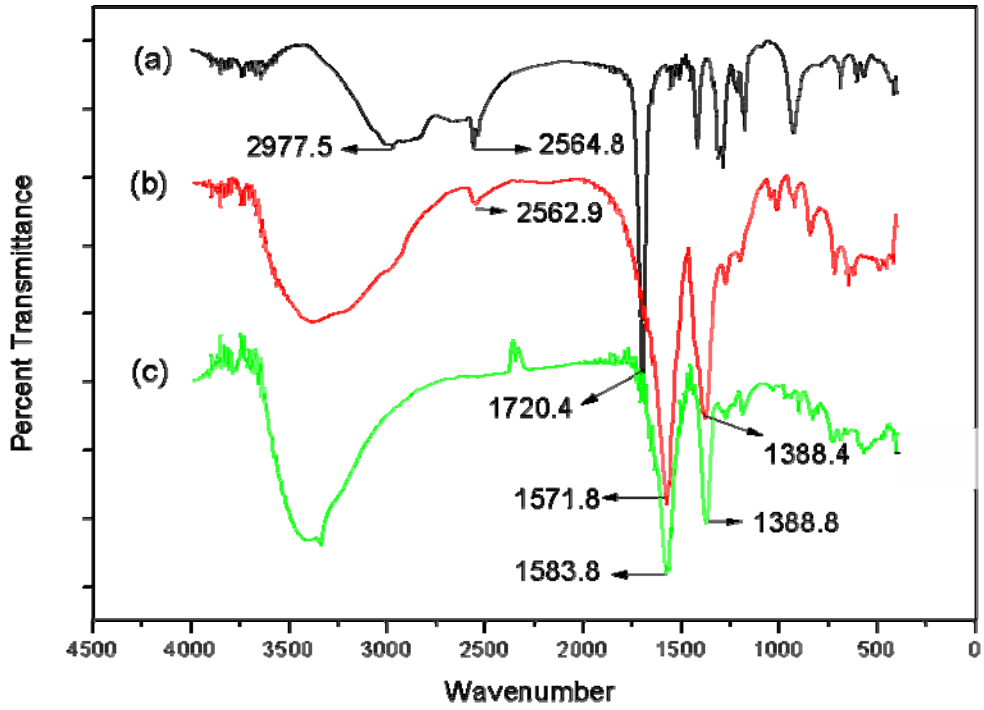

Figure 3.2 FT-IR spectra of (a) DMSA, (b) Cd-DMSA complex formed at pH 7.5 and room temperature (RT) (c) DMSA coated CdS QDs (ES24G) formed at pH 7,5 and 70ºC

3.1.2 Effect of Temperature and pH on particle formation and properties

Reaction temperature and pH are usually important reaction variables to consider. Acidic pH range is not suitable for these reactions due to the protonation of carboxylic acid and thiol groups which are responsible from the solubility and stability of nanocrystals. Moreover, it was reported that Cd^{2+} ions are not complexed with a thiolated ligand at pH<4.0[57]. Cd-DMSA complex becomes soluble at pH 7.0 and so, reaction pH should

better be higher than 7.0. If reactions are performed at room temperature, formation of luminescent CdS QDs could be achieved at pH values higher than 8.5 in a reasonable time. However, as the pH increased, larger size particles were formed. Furthermore, pH values of 11.0 and higher caused nearly non-luminescent or bulk QDs. At basic pH values HS^- concentration decreases (for H_2S, pKa_1 = 7.0, and $pKa_2 \approx 19.0$[58]) and mostly S^{2-} contributes to the CdS formation yielding faster crystal growth.

Influence of reaction temperature is more dramatic. The minimum required temperature for sulphur release at pH 7.5 is 50 ºC as only at this temperature CdS QDs were formed. Even at pH 8.0 an immediate formation of bulk CdS was observed at high temperature values (≥50°C). The limiting reaction conditions and corresponding reaction times are summarized in Table 3.1.

Table 3.1 Temperature and pH values at which colloidal CdS QD could be synthesized and resulting reaction times

T (ºC)	pH	Reaction time
RT	8.5 - 11.0	≥ 1 day
≥ 50 ºC	7.5 - 8.0	≤ 2 hours

Since low temperatures yielded significantly low quality CdS QDs in long reaction times, CdS formation via DMSA decomposition was carried out at moderate temperature, 70ºC, for the study of other parameters. At this temperature, pH value of 7.5 was prefered in order to achieve controlled synthesis of CdS QDs. This pH value is also beneficial for bioapplications of these QDs.

3.1.3 Effect of the SH/Cd Ratio on particle formation and properties

Since DMSA has a dual function as the sulfur source and the stabilizer in our CdS QD synthesis, the SH/Cd ratio is a very essential parameter affecting the properties of the QDs. Furthermore, Cd/S ratio and ligand concentration have been reported to have significant role on the size and properties of QDs coated with thiolated molecules[39]. DMSA capped CdS nanocrystals with the decomposition of DMSA were studied at different ratios of SH/Cd as summarized in Table 3.2.

Table 3.2 SH/Cd ratios used in the synthesis of CdS QDs and Particle properties

Sample ID	SH/Cd (mol ratio)	Abs. cutoff (λ) (nm)	PL max. (nm)	size[a] (nm)	band gap[b] (eV)	fwhm[c] (nm)	QY[d] (%)
ES24B	1.5	350	453	2.1	3.55	125	-
ES24C	2.0	369	447	2.3	3.36	110.5	-
ES24D	2.5	400	472	2.6	3.10	132	8.5
ES24G	2.7	410	504	2.7	3.03	143	8.9
ES24	3.0	417	522	2.8	2.98	146	7.9
ES24E	3.5	416	519.5	2.8	2.98	148.5	7.9
ES24F	7.0	437	557.5	3.1	2.84	148	6.2

[a]Calculated by by Brus effective mass approximation[15]. [b]Corresponding band gap energy calculated by E=hν. [c]Full-width at half-maximum calculated from PL spectra. [d] QY calculated according to the procedure of [19] by using Rhodamine B as a reference (31% QY in water)

In Figure 3.3(A, B), the UV-vis and PL spectra of CdS QDs prepared at different SH/Cd ratio are shown. A red shift for absorption and emission peaks is evident with the increasing DMSA amount. At SH/Cd ratios of 1.5 and 2, luminescent CdS quantum dots

could not be obtained. Probably, DMSA amount was not sufficient both as a S^{2-} supply and for the stabilization of the forming crystal. Further increase in the SH concentration yields slightly larger particles that luminesce (Table 3.2). Increasing DMSA amount supplies higher concentration of sulfide ion for growth and more DMSA for coating. After the SH/Cd ratio was raised above 7, bulk CdS was obtained rapidly at given reaction conditions (pH=7.5, 70°C). Sizes of the crystals were tuned from 2.6 nm to 3.1 nm by changing the SH/Cd ratio from 2.5 to 7. Quantum efficiencies were calculated as around 8-10 % with respect to Rhodamine B. Figure 3.3C illustrates the transparent solutions of these nanoparticles in ambient conditions and the emissions of CdS QDs from blue to orange under excitation (365 nm). The reaction time for ES24D(SH/Cd=2.5) was around 5 hours but above this ratio, it took around 1 hour due to the more interaction of S^{2-} with Cd^{2+} with higher amount of sulfur release. Size of the crystals could also be increased further by increasing the reaction time.

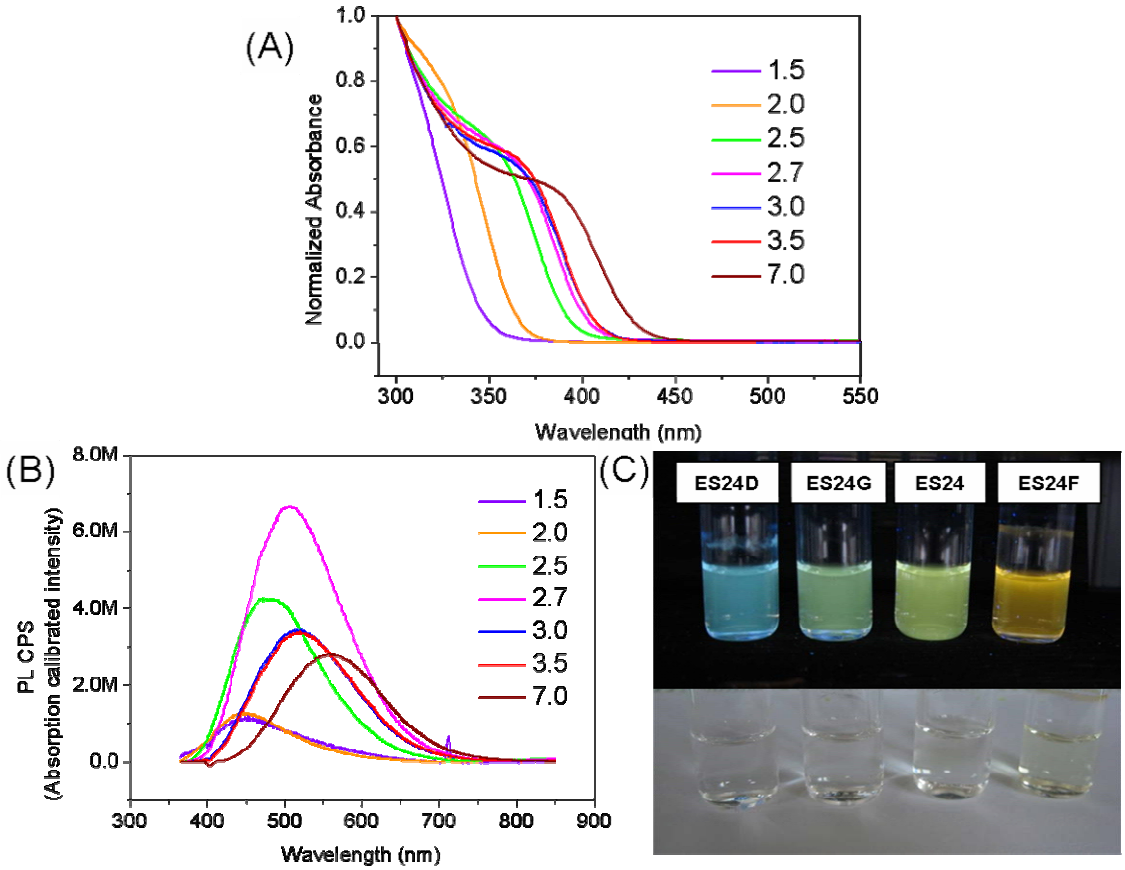

Figure 3.3 The evolution of the peak positions of absorbance (A) and, corresponding emission (B) spectra of CdS QDs at different SH/Cd molar ratios. The excitation wavelength was 355 nm. The photograph of aq. CdS under daylight (bottom) and UV excitation at 365nm (Top) (C). All particles were prepared at pH=7.5, 70ºC.

3.1.4 Stability

The stability of CdS QDs was investigated under different storage conditions for several days. Two samples were washed by 3K ultrafiltration device to remove excess materials and two samples were kept as they were synthesized. One washed and unwashed sample

were kept at room temperature (exposed to daylight) and the other two were stored in the refrigerator. The UV-vis and PL spectra of these four samples are shown in Figure 3.4. It is clearly seen that size didn't change when samples were stored in the fridge. PL intensities remained unchanged for the unwashed but increased slightly for the washed sample. On the other hand, ambient conditions first caused a slow disappearance of the first excitonic peak from the absorption spectra and then a slight red shift on the absorption edge corresponding to a size increase. More importantly, luminescence decreased after 10 days followed by a precipitation after 15 days. Slow decomposition of the DMSA could cause a slow growth of the particles through Oswald ripening but more importantly slow detachment from the surface which would lead into aggregation and finally to precipitation.

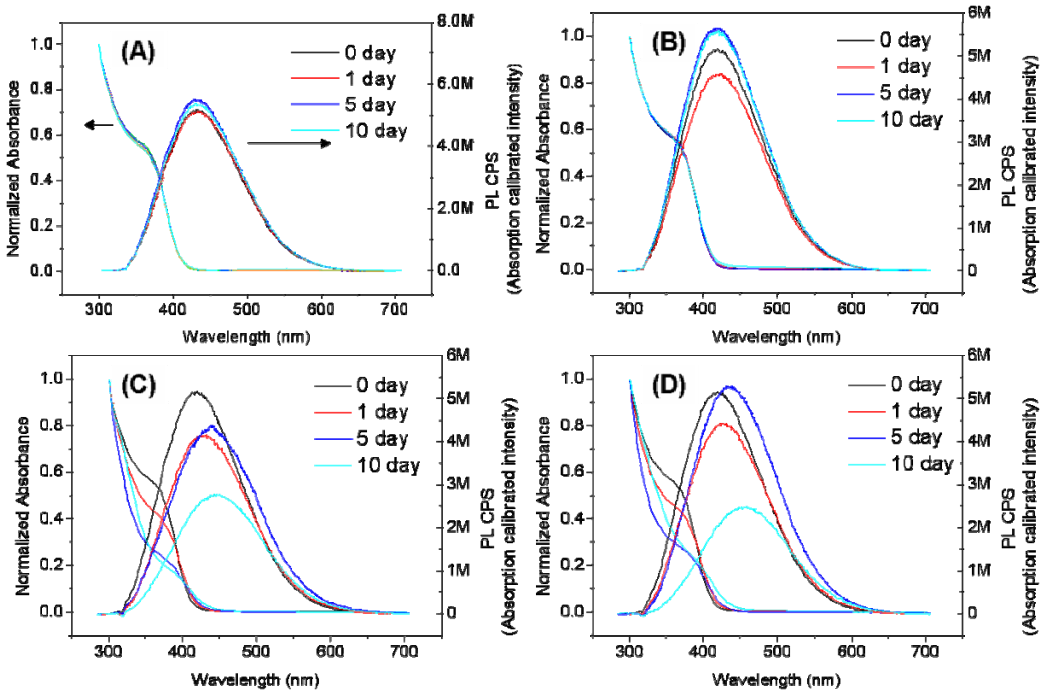

Figure 3.4 UV-vis and PL spectra of (A) unwashed, (B) washed QDs stored in refrigerator and (C) unwashed, (D) washed QDs kept under ambient conditions

3.2 CdTe/CdS core/shell nanoparticles

3.2.1 Synthesis of CdTe/CdS core/shell QDs by the decomposition of DMSA

Synthesis of CdTe was performed in water with Na_2Te as the Te^{2-} source; Na_2Te was prepared with 100% purity. Figure 3.5 shows the XRD pattern of Na_2Te which fits perfectly to the theoretical values.

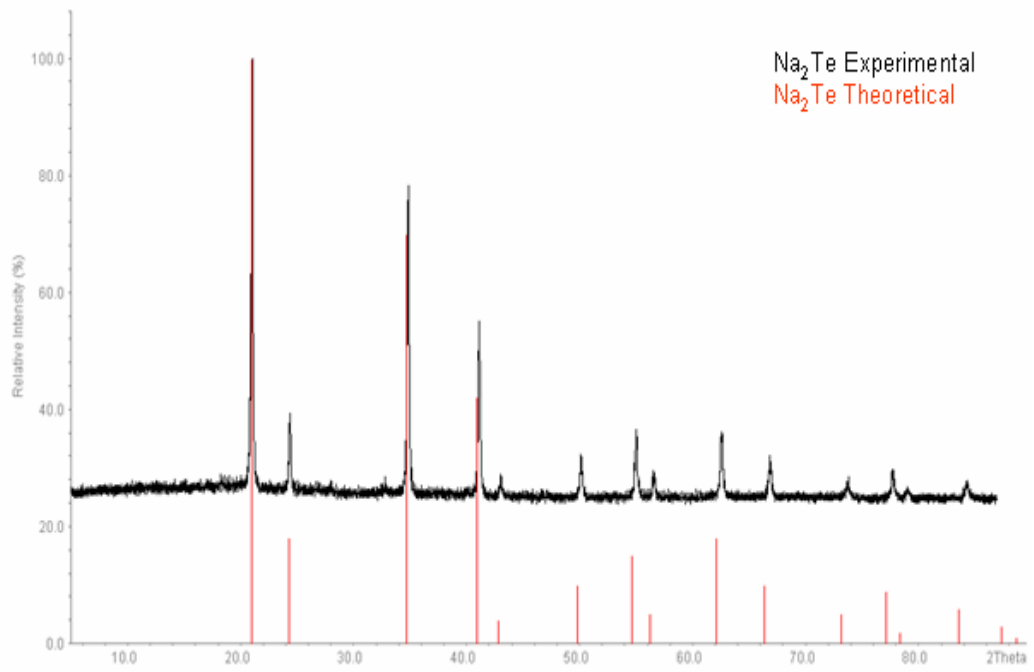

Figure 3.5 XRD pattern of synthesized Na_2Te.

The CdTe/CdS core/shell QD synthesis begins with the addition of DMSA to the CdTe QD reaction solution. CdTe crystals were capped with 2MPA. Excess amount of Cd^{2+} with respect to Te^{2-} exists in this solution. Therefore, the slow release of S^{2-} from DMSA results in the growth of CdS shell around the CdTe forming CdTe/CdS core/shell structure.

XRD indicates (Figure 3.6) a CdS shell formation around CdTe QDs. XRD peaks of CdTe-2MPA fits to the zinc blende structure of CdTe. However, these peaks shift towards CdS in the CdTe/CdS QDs. There are no free CdS QDs in the sample since there are no peaks fitting to CdS structure in the XRD pattern. Therefore, we believe that the epitaxial growth of CdS on CdTe was achieved. These XRD peaks are rather broad because of their extremely small size.

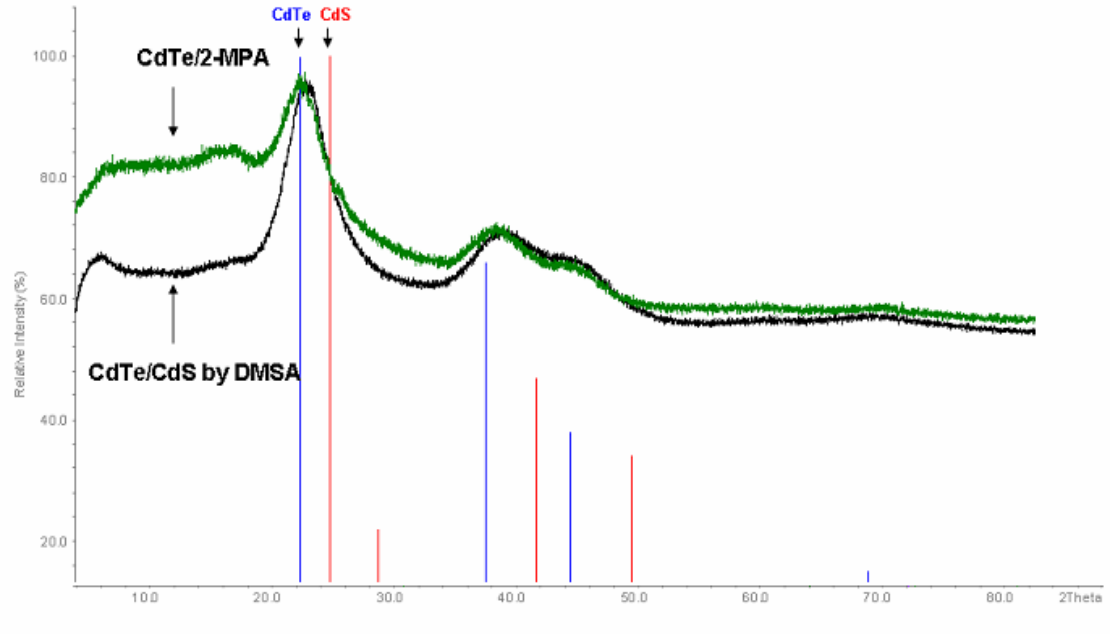

Figure 3.6 XRD pattern of CdTe/CdS core/shell nanocrystals prepared by DMSA. The lines correspond to bulk cubic zinc blende CdTe and CdS

An important finding here is that DMSA did not replace 2MPA from the CdTe core, at least not completely. FTIR spectra in Figure 3.7 shows aliphatic C-H stretching peaks of the 2MPA for both CdTe-2MPA and CdTe/CdS-2MPA/DMSA species.

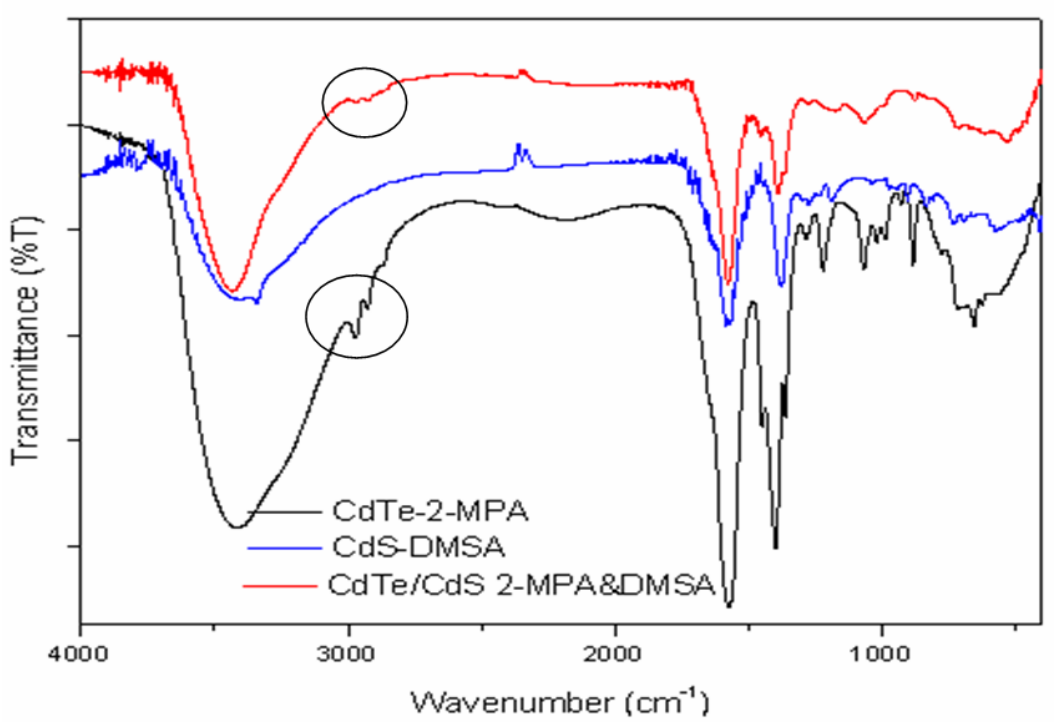

Figure 3.7 FTIR spectra of CdS-DMSA, CdTe-2-MPA and CdTe/CdS-2MPA/DMSA QDs

3.2.2 Influence of the SH(DMSA)/Cd(initial) ratio

The reflux time has a significant influence on the size and QY of the CdTe nanoparticles. Due to the confinement effect in QDs, particle size determines the wavelength of light absorbed and emitted. Figure 3.8 indicates change in the size and QY as a function of time for CdTe-2MPA. As the reflux time is prolonged, the absorbance edge (Figure 3.8(A)) and PL max (Figure 3.8(B)) continuously shifted towards longer wavelengths, meaning, larger particles are formed by Oswald ripening.

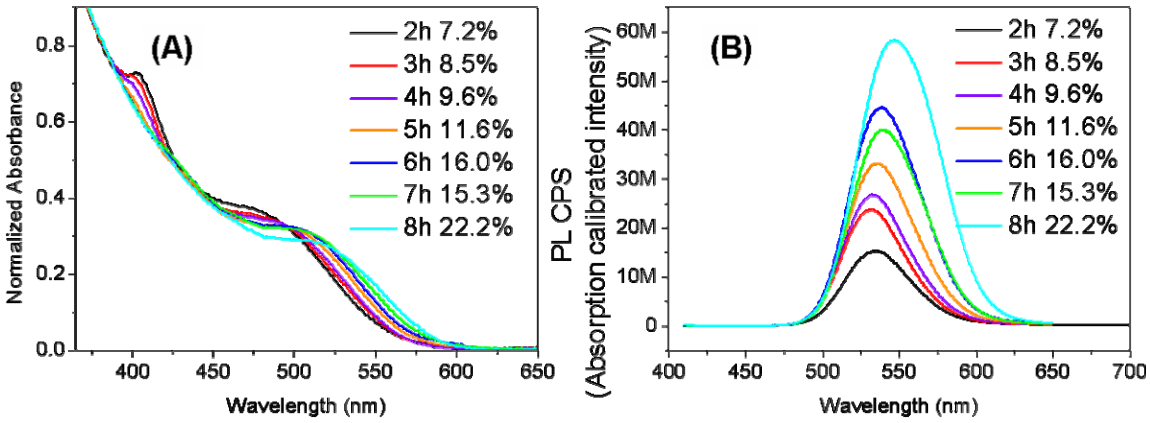

Figure 3.8 UV-vis (A) and PL (B) spectra of 2-MPA stabilized CdTe QDs. The excitation wavelength is 400 nm. Cd^{2+}:Te^{2-}:SH=1:0.38:2.4, pH=9 and T=90ºC

A CdS shell formation on the CdTe core was initiated by the introduction of DMSA to the CdTe reaction solution. During the reflux, the slow release of S^{2-} via decomposition of DMSA caused the growth of CdS shell around CdTe by the reaction with excess Cd^{2+}. Therefore, longer reflux times results in thicker shell around the core. Of course, since no additional Cd^{2+} was introduced, the thickness would be limited. For the synthesis of CdTe/CdS core/shell QDs, three SH (DMSA)/Cd(initial) molar ratios were performed to investigate the effect of the amount of DMSA on the CdS shell formation and luminescence properties of these particles. The absorbance spectra of CdTe/CdS core/shell QDs prepared with the SH (DMSA)/Cd ratio of 0.5, 0.7 and 1.0 are presented in Figure 3.9(A, B and C). As expected, the absorbance edge and PL_{max} shifted to longer wavelengths with prolonged reflux time. However, in this case, the absorbance edge and PL max are red-shifted with respect to CdTe core due to the CdS shell formation. Moreover, the CdTe/CdS QD solution color changed from light orange to brown during the reflux.

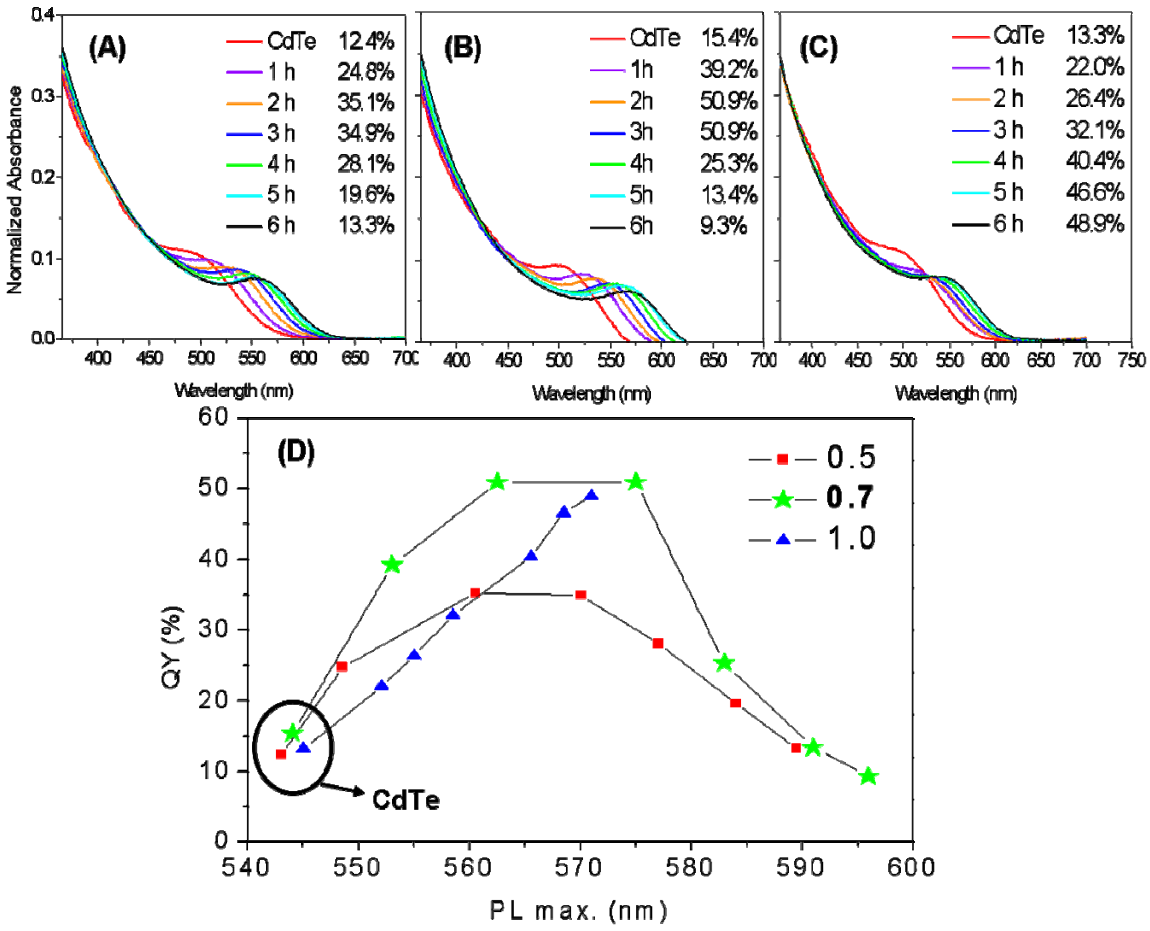

Figure 3.9 Absorbance spectra of CdTe/CdS core/shell QDs prepared by the decomposition of DMSA at SH(DMSA)/Cd(initial)=0.5 (A), 0.7 (B) and 1.0 (C). Change in QY with $PL_{max.}$ shift during reflux at SH(DMSA)/Cd(initial)=0.5, 0.7 and 1.0 (D). $\lambda_{exc.}$=400 nm. Cd^{2+}:Te^{2-}:SH(2-MPA)= 1.0:0.38: 2.4, pH=9 and T=90ºC

Figure 3.9(D) illustrates the QY change at these ratios with increasing PL_{max} as the reaction proceeds. More or less all CdTe-2MPA QDs have similar QY before shell formation. As the CdS shell grew on the CdTe core, QY increased gradually at all ratios reaching to a maximum value and then declines again. In case of the SH (DMSA)/Cd ratio

of 0.7, QY was increased from 16% to a 51% by the epitaxial growth of the CdS shell. This increase is attributed to the removal of surface defects and dangling bonds causing non-radiative recombination on the surface, and to the smoothing the core surface (CdTe) by the help of a larger band gap semiconductor (CdS) [8]. Decreasing luminescence after reaching to a maximum value might originate from the formation of surface defects by greater lattice mismatch between CdTe and CdS materials with the thickening of CdS shell and new defects formed on the CdS surface[8]. The removal of capping material from the CdTe/CdS core/shell QD surface at longer reflux time might also be a secondary reason as it was also seen in the case of CdTe core.

SH (DMSA)/Cd ratio of 1.0 provided a substantial improvement in the QY as seen in Figure3.9 (D); however, large black precipitates were formed in these reactions possibly due to the excess DMSA and the QY increase was not as high as the case with 0.7 ratio. When the SH(DMSA)/Cd ratio was dropped down to 0.5, maximum QY of QDs reached was only 35.1%, possibly due to the lack of enough DMSA for an effective coating. Therefore, 0.7 was chosen as the optimum molar ratio for the formation of an effective CdS shell around CdTe core under these conditions.

3.2.3 Comparison of DMSA with Thioacetamide (TAA) as a sulfur source

Thioacetamide is widely used for the shell formation via slow release of sulfide ion in the literature [11, 33]. In order to evaluate the efficiency of DMSA as a shell forming material, CdS shell was grown on CdTe-2MPA core by thermal decomposition of TAA at exactly the same ratios and procedure used for DMSA. The SH (TAA) /Cd (initial) ratio of 0.7, which is the optimum SH (DMSA) /Cd (initial) ratio, was applied. Figure 3.10 illustrates the optical properties of CdTe/CdS core/shell nanoparticles obtained by using TAA and DMSA as the S^{2-} source. Figure 3.10(A) and (B) shows that they have similar affinity to have larger particles at longer reflux time. However, at the same time intervals,

larger particles meaning thicker CdS shell was formed by the TAA compared to DMSA. This indicates much faster release of S^{2-} from TAA than that of DMSA.

On the other hand, the QY of core/shell particles could increase up to only 26.5% which is nearly the half of the values achieved with the DMSA (Figure 3.10(C)). This made us believe that the surface capping of DSMA could be responsible for this exceptional improvement in the QY which can not be achieved by the TAA. According to us, there still exists the second thiolate group of DMSA in the reaction solution which contributes to 2-MPA for the passivation of CdTe/CdS core/shell surface. Moreover, slow sulphur release from DMSA might cause better crystallinity of CdS shell which resulted in higher QY value than TAA case. Of course when absence of a second capping molecule in case of TAA reaction is considered as the crystal grew, existing 2MPA was supposed to provide passivation of the new surface, which is probably not enough, leaving behind defects which are detrimental for the quantum efficiency.

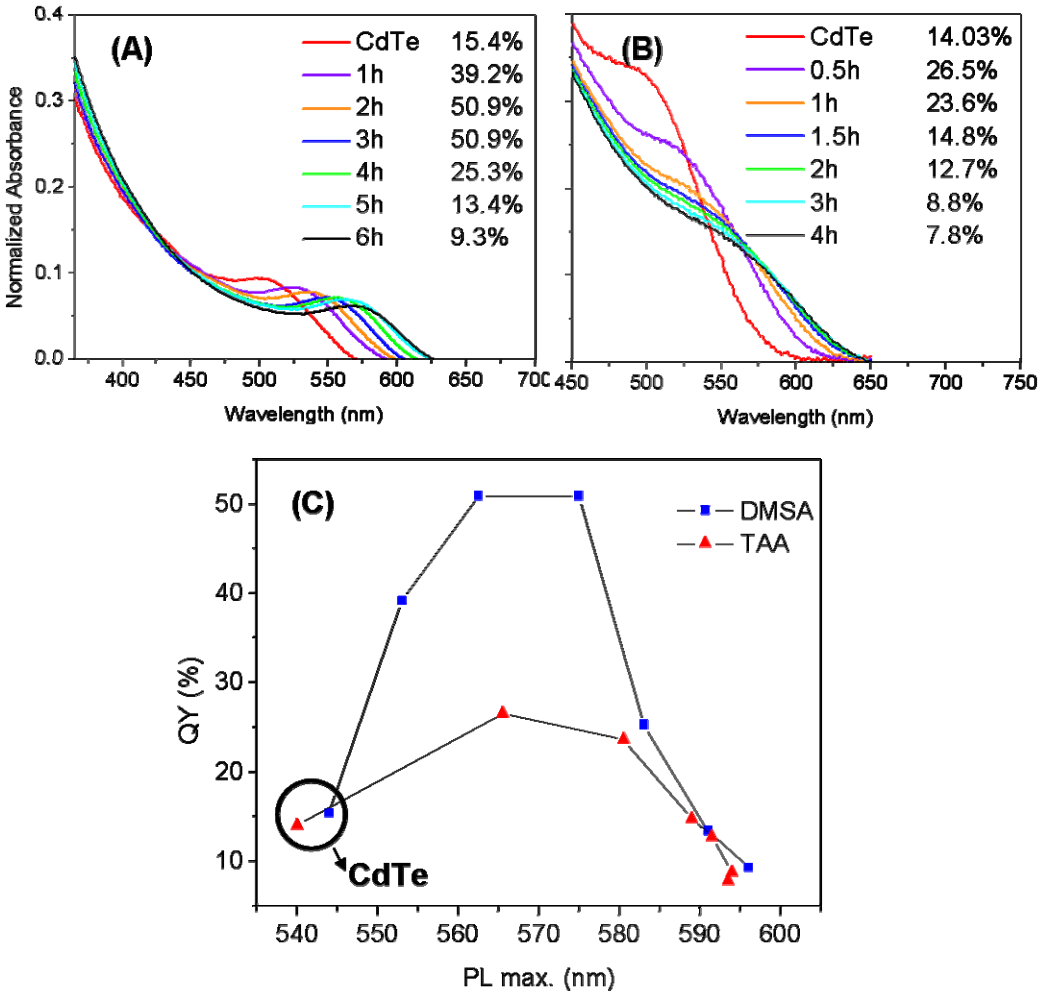

Figure 3.10 UV-vis absorbance spectra of CdTe/CdS QDs prepared by the decomposition of DMSA (A) and TAA (B). QY change with PL max. shift during reflux, TAA vs. DMSA (C).The excitation wavelength is 400 nm. SH(TAA)/Cd(initial)=0.7, pH=9 and T=90ºC

The CdTe/CdS core/shell structure was further confirmed by XRD measurement. In Figure 3.11, it is clearly seen that peaks are located between the theoretical values of CdTe and CdS cubic zinc blende crystal structures.

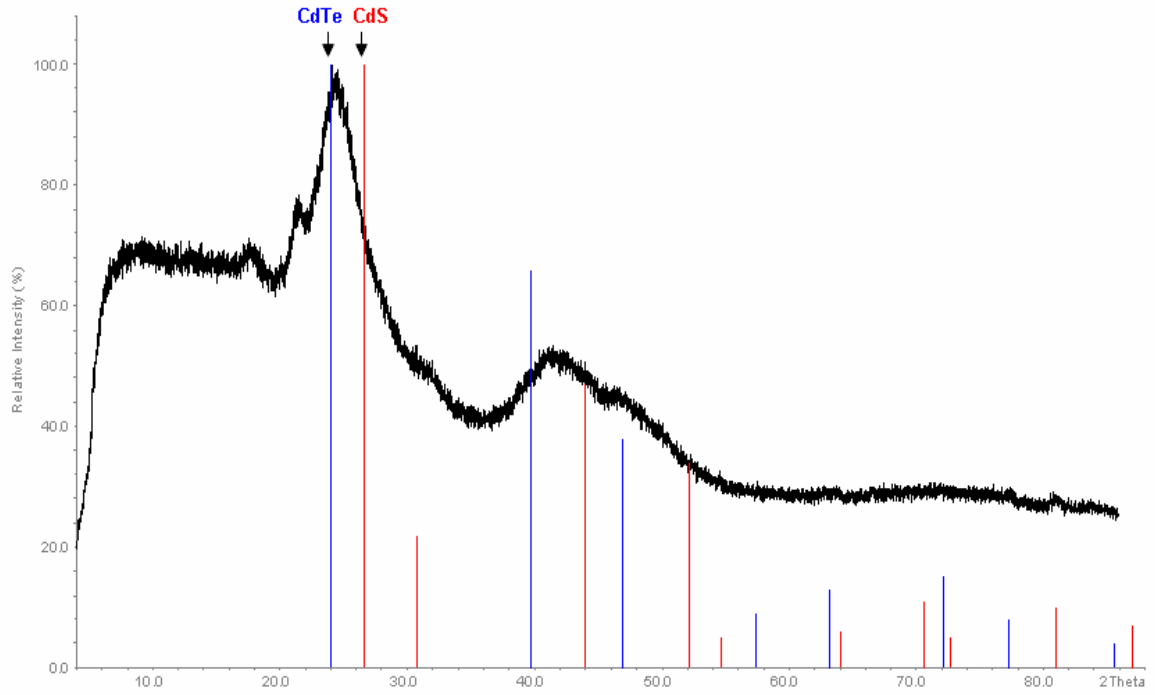

Figure 3.11 XRD pattern of CdTe/CdS core/shell nanocrystals prepared by TAA. The lines correspond to bulk cubic zinc blende CdTe and CdS

3.2.4 Influence of pH on particle properties

The pH value of the reaction is an important factor influencing the growth and the luminescence behavior of thiol-capped QDs. [27, 39, 57-59]. Therefore, the influence of pH on the particle properties, mainly QY, was studied for the CdTe/CdS core/shell QDs. One objective of this specific investigation is to find the best pH value for the highest luminescence obtained from the CdTe core as well. Initially, Cd^{2+}:Te^{2-}:SH(2-MPA) ratio was fixed at 1:0.38:2.4 and the initial pH was set to 7.5, 9.0 and 11.0. Later, DMSA was added at the optimum SH (DMSA)/Cd (initial) ratio of 0.7. Initial pH is the pH value of the reaction solution before the addition of telluride. UV-Vis absorbance spectra of CdTe and CdTe/CdS QDs prepared at these pH values are illustrated in Figure 3.12(A), (B) and

(C), respectively. Initial pH mainly affected the QY and the growth rate of QDs. Figure 3.12(D) shows that QY decreased with the increasing pH. QY of the CdTe core dropped from 19% at pH 7.5 to 15% at pH 9 and to 3% at pH 11. Maximum QY achieved for the CdTe/CdS core/shell QDs was 73%, 51% and 10% for pH 7.5, 9.0 and 11.0, respectively. Furthermore, ability to tune the size of the CdTe/CdS core/shell QDs can only be achieved at pH 7.5 providing particles luminescing from green to red (Figure 3.12 (E)). The growth rate was accelerated at higher pH values resulting in bulk material in a shorter time period. In Figure 3.12(D) indication of such enhanced growth rate can be seen easily: at pH 11, after only two hours PL intensity decreases and shortly after bulk material was formed.

Complexation of excess cadmium and thiol during the synthesis of QDs is reported to be dependent on the pH of the solution [57, 58, 60]. In these reactions, initial pH mainly affects the quality of CdTe core demonstrated with a decreasing QY with increasing pH. The structures of the possible complexes prior to the formation of nanoparticles and later at the surface of the particles are reported to be different at different pH values, resulting in a change in the surface properties of core QDs. In addition, Figure 3.12 (D) illustrates that shell growth around these particles could improve their quality. Growing a CdS shell on these particles tripled the QY at all pH values. There is an important point to be highlighted here; The pH values of the CdTe reaction solutions before DMSA addition (before shell growth) were very close (around 9.0) despite having different starting pH values. Therefore, it was concluded that this dramatic QY difference between these core/shell QDs was resulted only from the initial pH effect on the quality (structure of complexation, surface property) of the core QDs. The formation of CdS shell around the core QD only helped further improvement of surface passivation and stability.

From the previous study of CdS synthesis by the decomposition of DMSA, it is known that higher pH values cause larger particles. Therefore, it was expected to have a thicker CdS shell at pH 11.0 than 7.5. UV- Vis absorbance spectra and PL max. shift of CdTe/CdS

core/shell QDs in Figure 3.12 shows that the shell growth rate was much higher at pH 11 than pH 7.5 as expected. Bulk CdTe/CdS core/shell QDs were achieved in a very short reflux time at pH 11.0. The fast growth causes low crystallinity and more defects on the surface and interface [61]. Larger lattice mismatch between CdTe and CdS appears as the CdS shell thickens, as well. Yet, lowering the pH allows good quality CdTe/CdS core/shell QDs luminescing in a wide range of spectrum. In bio-applications, having red luminescent QDs with high QY is significant for imaging to eliminate absorption by the tissue at lower wavelengths. Therefore, pH 7.5 is the optimum pH for CdTe/CdS core/shell QDs.

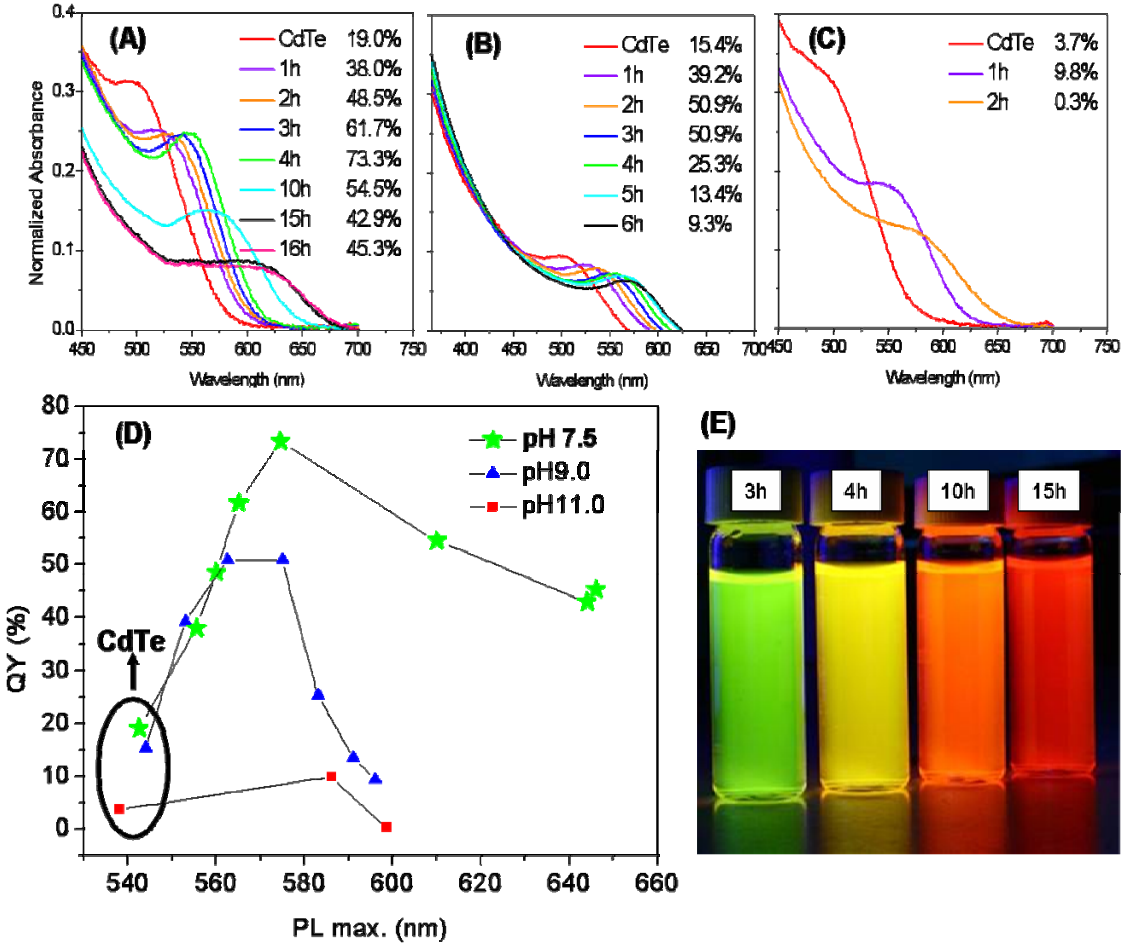

Figure 3.12 UV-vis absorbance spectra of CdTe/CdS core/shell QDs prepared by the decomposition of DMSA at initial pH=7.5(A), 9.0 (B), 11.0(C). QY change with PL max. shift during reflux at pH=7.5, 9.0 and 11.0 (D) The excitation wavelength is 400 nm. The photograph of CdTe/CdS solutions at different sizes under 365nm UV-lamp excitation. The raction times are indicated on each solution (E). Cd^{2+}:Te^{2-}:SH(2-MPA)= 1.0:0.38: 2.4, Cd^{2+}: SH(DMSA)=1.0:0.7, and T=90ºC

3.2.5 SH(2-MPA)/Cd(initial)

Optimization of the CdTe core would improve the properties of the CdTe/CdS core/shell QD. ligand concentrations known to be influential on the physical and chemical properties of QDs[39, 59]. So, at the optimum SH (DMSA)/Cd (initial) ratio 0.7 and initial pH 7.5, 2-MPA amount was varied: SH (2-MPA)/Cd (initial) ratio of 1.5, 2.4 and 5.0 were applied. Figure 3.13(A), (B) and (C) illustrates UV-Vis absorbance spectra of CdTe and CdTe/CdS core/shell QDs prepared at these ratios, respectively. Here, growth of the core/shell QDs is clearly seen by the red shift with reflux time. The experimental data in Figure 3.13(D) show that decreasing , increased the QY of the CdTe core l(4.6% at ratio=5.0, 19.0% at ratio=2.4 and 30.5% at ratio=1.5) but did not impact the particle size significantly. The best QY for CdTe/CdS core/shell was achieved at the ratio 2.4 (73.3%) and highly green to red luminescent CdTe/CdS core/shell QDs could only be obtained at this ratio (Figure 3.12(E)).

First of all, ligand/Cd ratio should be minimum 1 to have sufficient amount of stabilizer which provides stability and surface passivation of QDs. It was reported for the TGA (L^{2-}) capped CdTe QDs that as the ratio approaches to 1, Cd(L) complex concentration increases ($Cd(L_2)^{2-}$ decreases and $Cd(L_3)^{4-}$ disappears) resulting in better surface quality and high QY at the initial stages of the synthesis[59]. Therefore, the increase in QY of CdTe core QDs is reasonable according to this study. However, QY change of core/shell QDs does not follow the same trend. It is illustrated in Figure 3.13 that maximum QY (73.3%) and wider range of color emission (from green to red) was achieved at SH (2-MPA)/Cd (initial) ratio of 2.4. The ratio of 1.5 and 5.0 gave 58.4% and 38.6% QY, respectively, and maximum orange emission was obtained through these reactions. The reason behind QY decrease and faster precipitation during the synthesis at the ratio of 1.5 may be the deficiency of 2-MPA to stabilize the growing CdS shell around the core QD. As the size of the particle increases, more stabilizers are needed for the passivation of the surface dangling bonds and defects.

Therefore, the ratio of 1.5 could not provide the needed amount of 2-MPA at the former stages of the reaction. On the other hand, QY decrease at the ratio of 5.0 was an expected result which might be caused from the initial complexes ($Cd(L_3)^{4-}$) formed during CdTe core synthesis. Although the CdS formation improved the surface quality of CdTe QDs by increasing their QY from 4.6% to 38.5%, the efficiency of CdTe/CdS core/shell quantum dots could not reach the ratio of 2.4. Therefore, Cd^{2+}:Te^{2-}:SH(2-MPA)=1:0.38:1.5 was chosen as the optimum ratio for 2-MPA capped CdTe QDs but Cd^{2+}:Te^{2-}:SH(2-MPA)=1:0.38:2.4 was the best for 2-MPA capped CdTe/CdS core/shell QD synthesis.

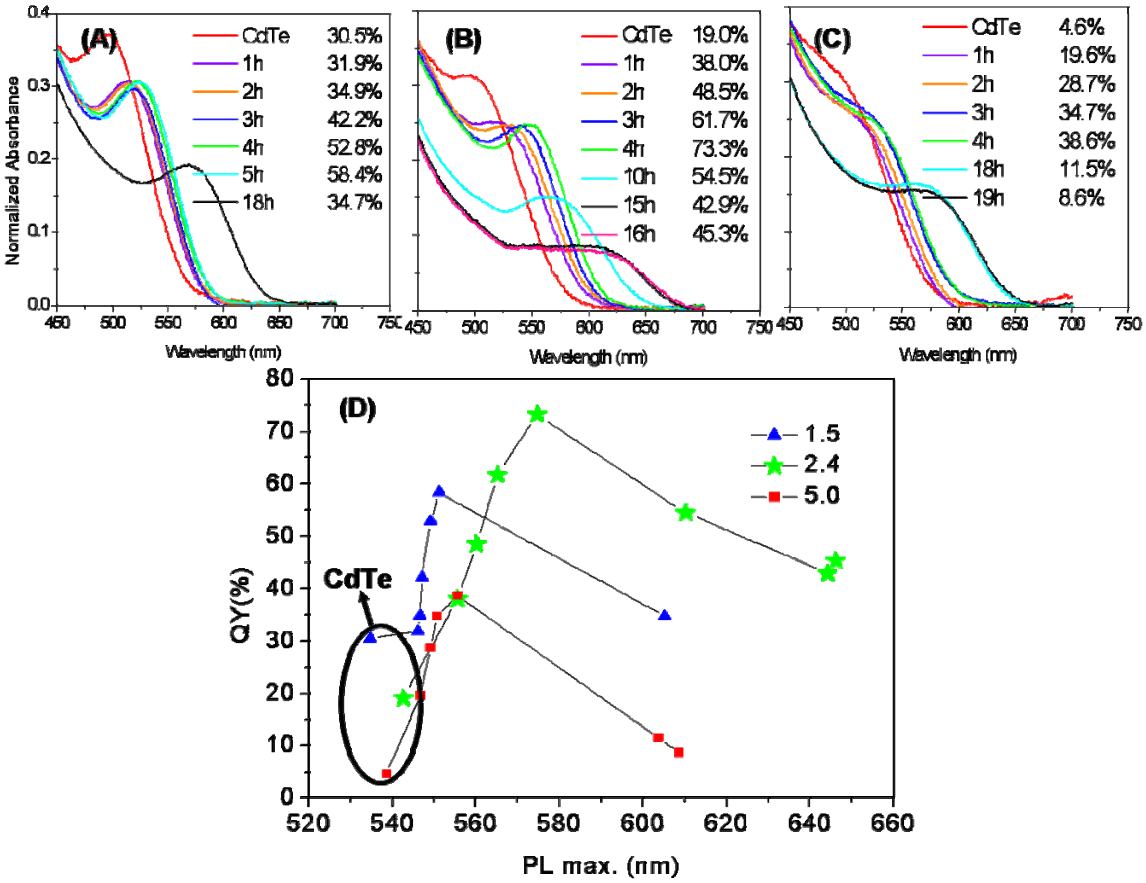

Figure 3.13 UV-vis absorbance spectra of CdTe/CdS core/shell QDs prepared by the decomposition of DMSA at Cd^{2+}: SH(2-MPA)= 1.0: 1.5 (A), 2.4 (B), 5.0 (C). QY change with PL max. shift during reflux at Cd^{2+}: SH(2-MPA)= 1.0: 1.5, 2.4, 5.0 (D). The excitation wavelength is 400 nm. Cd^{2+}: Te^{2-}= 1:0.38, Cd^{2+}: SH(DMSA)=1.0:0.7, initial pH= 7.5 and T=90ºC

3.2.6 Stability

The photostability of 2-MPA capped CdTe and CdTe/CdS core/shell QDs was examined to understand their behavior in ambient conditions. In Figure 3.14, the UV-Vis

(A) and PL (B) spectra of CdTe QDs aged under daylight are presented. Both absorbance edge and PL max experienced obvious blue shift which is a result of shrinkage of particles. The reason behind this decrease in size may be the oxidation of Te^{2-} in the CdTe crystals because they are known to be oxidized easily. Simultaneously, it is seen that the QY of CdTe QDs was enhanced from 5.6% to 32.5%. The irradiation might cause decomposition of 2-MPA leading to the growth of CdS shell around CdTe by the release of sulfur. This process might result in QY increase in 13 days of irradiation. Here, the oxidation might proceed much faster than the CdS shell growth, so that blue shift of 18 nm couldn't be avoided. After a critical CdS shell growth by further decomposition of 2-MPA, the oxidation might be prevented and so that the particle size started to increase. After a month, the degradation process might bring about the lack of capping agent for the stabilization of QD surface and solubility, causing decrease in QY and the formation of precipitates at the end. However, these precipitates are not bulk CdTe because they are still green-yellow luminescent.

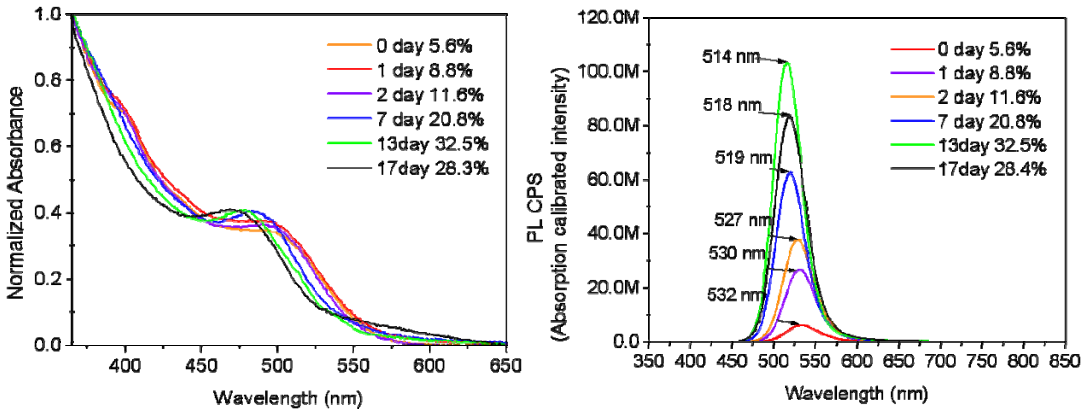

Figure 3.14 UV-vis (A) and PL (B) spectra of 2-MPA stabilized CdTe QDs under ambient conditions. The excitation wavelength is 400**.**

Figure 3.15 illustrates the UV-Vis (A) and PL (B) spectra of daylight irradiated CdTe/CdS core/shell QDs. In contrast to CdTe core QDs, neither the absorbance edge nor the PL max shift, meaning, the oxidation of Te^{2-} was successfully prevented by the formation CdS shell around the CdTe core during the reaction. Moreover, further photodegradation of DMSA and 2-MPA did not lead to an increase in the CdS shell thickness. However, the QY of CdTe/CdS core/shell QDs increased to a maximum value of 70% in 12 days. After that point, the decrease of QY and colloidal instability started; which might be a result of deficiency of the capping agent by further decomposition.

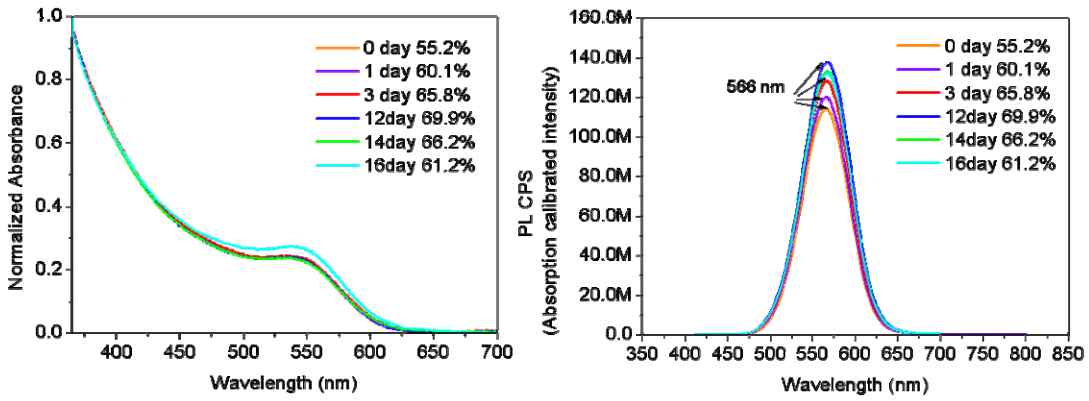

Figure 3.15 UV-vis (A) and PL (B) spectra CdTe/CdS core/shell QDs prepared by decomposition of DMSA under ambient conditions. The excitation wavelength is 400 nm.

3.2.7 Fluorescence lifetime

Luminescence lifetimes of the CdTe/CdS QDs could give further information about CdS growth on CdTe core. . In Figure 3.16, the PL decay curves of the 2MPA-capped CdTe and 2MPA&DMSA-capped CdTe/CdS core/shell nanocrystals are illustrated. Here, the improvement of fluorescence lifetime of with the CdS shell formation is clearly

observed. However, a deeper investigation is also needed. PL decay curve of each sample has a biexponential form of

$$A_1 \exp\left(\frac{t}{\tau_1}\right) + A_2 \exp\left(\frac{t}{\tau_2}\right) \tag{3.1}$$

where τ_1 is the shorter lifetime component usually equal to several nanoseconds and τ_2 is the longer lifetime component of several tens of nanoseconds. The shorter lifetime corresponds to the intrinsic recombination of initially populated core states, and the longer lifetime is attributed to radiative recombination of carriers at the surface states according to the literature reports[62]. The parameters A_1 and A_2 represent the amplitudes of the slow and fast decay components on a percentage basis.

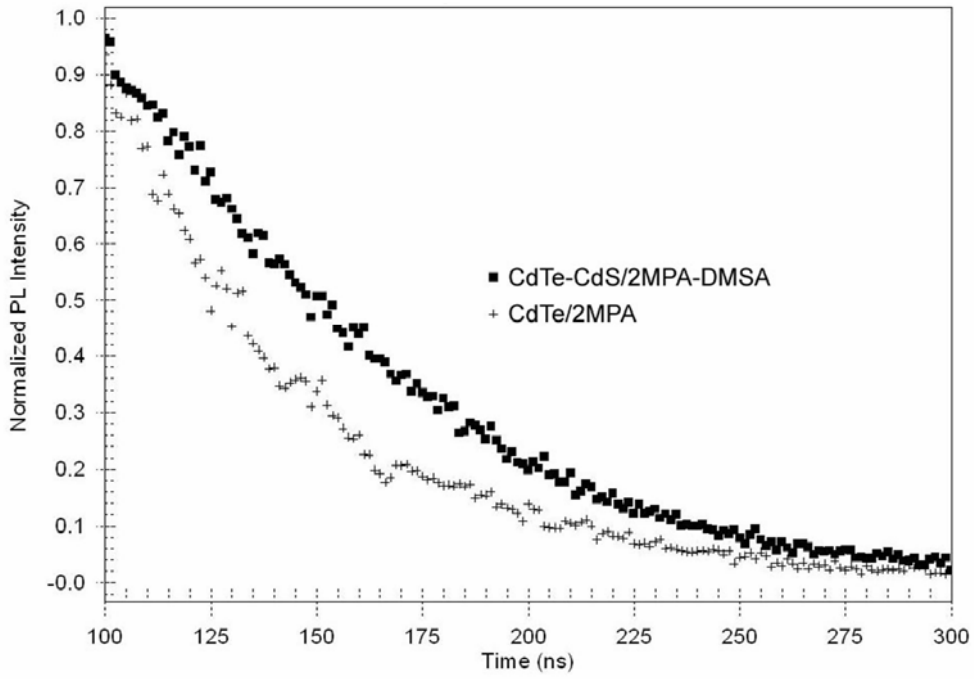

Figure 3.16 PL decay curves (λ_{ex}=400 nm) of CdTe and CdTe/CdS core/shell QDs at RT in water

Table 3.3 lists the parameters of Eqn. (3.1) for the CdTe and CdTe/CdS core/shell samples. There is a great difference between the core and the core/shell nanocrystals. The first one is that both τ_1 and τ_2 values of CdTe/CdS (8.6 and 48.2 ns) are much larger than that of CdTe (1.7 and 25.3 ns). The radiative recombination in the core states is increased around 4-fold and surface related recombination of carriers nearly doubled. This indicates that fluorescence lifetime of bare CdTe are significantly improved by the epitaxial growth of CdS shell.

Table 3.3 Parameters derived by fitting Eqn. 3.1

	A_1(%)	**τ_1(ns)**	**A_2(%)**	**τ_2(ns)**
CdTe	58.1	1.7	41.9	25.3
CdTe/CdS	39.4	8.6	60.6	48.2

The second difference is that, weight of the short lifetime component (A_1=58.1%) is larger than the longer lifetime component (A_2=41.9%) for CdTe which means that most of the radiative recombination of carriers occur at the core states because of the existence of surface defects causing non-radiative decays. However, longlifetime component becomes almost 61% when CdS shell is formed. This indicates that the trap sites at the surface of CdTe crystals are efficiently removed with CdS shell growth, providing better surface passivation compared to the organic surfactant 2MPA.

Chapter 4

CONCLUSIONS

4.1 CdS-DMSA Conclusions

CdS QDs were prepared through a novel and very simple procedure using meso-2, 3-dimercaptosuccinic acid (DMSA) both as a stabilizing agent and a sulfur source in a one pot reaction. DMSA was confirmed to give sulfur to the reaction solution resulting in the formation of luminescent CdS crystals. Moreover, it successfully acted as a water-soluble coating because we obtained stable suspensions of the QDs without any precipitation at the end of the reactions.

These experiments were carried out at different temperatures and pH. Reaction temperature of 70ºC and pH 7.5 came out as the optimum parameters. Since at high reaction temperatures, the decomposition of DMSA is accelerated, formation of large particles and bulk CdS and even precipitation is inevitable. At low temperatures, the crystallization cannot occur properly because of the slowness of the reaction. In addition, well controlled reactions couldn't be achieved at pH values higher than 8.0 because bulk CdS was formed immediately when DMSA was introduced to Cd^{2+} solution. Acidic pH range is not suitable for these reactions either since carboxylic acid and thiol groups would be protonated. Deprotonation of such groups are necessary for binding, stability, and solubility.

SH/Cd ratio played an important role in the CdS synthesis. Luminescent CdS quantum dots could not be obtained at SH/Cd ratios of 1.5 and 2. The deficiency of sulfur in the

reaction solution resulted in the formation of extremely small QDs that can not have effective luminescence. As the ratio was increased further, the increase in S^{2-} concentration provided larger size CdS nanocrystals which luminesce. Size increased with increasing concentration of the DMSA. However, after the ratio of 7, bulk CdS was obtained rapidly at these reaction conditions. Size of the CdS QDs was tuned from 2.5 nm to 3.1 nm by changing the SH:Cd ratio from 2.5 to 7. Quantum efficiencies of these particles luminescing from blue to orange were calculated as 8-10 % relative to Rhodamine B.

4.2 CdTe/CdS-2MPA/DMSA Conclusions

The simple fabrication of colloidal luminescent CdS QDs by the decomposition of DMSA inspired us to develop new materials by this approach. CdTe/CdS core shell structures were prepared by the decomposition of DMSA. It was known that core/shell structures yield better optical properties because of the removal of defects at the QD surface, prevention of non-radiative transitions and better confinement of excitons in the core. Here, we have chosen CdTe as the core material because it is widely used in bio-applications due to their emissions close to the NIR region.

The experiments were done in two steps but in a single pot. The first step was the synthesis of CdTe QDs stabilized by the 2-mercaptopropionic acid (2-MPA). In the next step, DMSA is added directly into the CdTe reaction solution and finally, CdS shell growth was achieved by the decomposition of DMSA. From the comparison of DMSA with a common sulphur source, TAA, it was concluded that slow sulphur release from DMSA caused better crystallinity of CdS shell and having extra thiol in its structure contributed to 2-MPA for the passivation of the core/shell surface. As a result, much better luminescence compared to widely used TAA case was obtained with DMSA. Influence of DMSA amount on the shell growth and luminescence properties were investigated. The SH(DMSA)/Cd ratio was varied (0.5, 0.7 and 1.0) at initial pH of 9.0 and Cd^{2+}:Te^{2-}:SH(2-

MPA)=1:0.38:2.4. Best results were obtained at the ratio of 0.7: QY rose gradually from 16% to a maximum value of 51%. The ratio of 0.5 and 1.0 could not yield better luminescence due to the lack and excess amount of DMSA, respectively.

Another variable studied was the initial pH of the reaction solution because it was known that the pH of the reaction is an important factor affecting the luminescence properties of thiol-capped QDs. At fixed (optimum) SH(DMSA)/Cd (initial) ratio of 0.7, and Cd^{2+}:Te^{2-}:SH(2-MPA)=1:0.38:2.4 initial pH was set to 7.5, 9.0 and 11.0. For both CdTe and CdTe/CdS QY decreased with the increasing pH. QY of CdTe was dropped from 19% at pH 7.5 to 15% at pH 9 and to 3% at pH 11 and maximum QY achieved for the CdTe/CdS core/shell QDs was 73%, 51% and 10% for pH 7.5, 9.0 and 11.0, respectively. Furthermore, size tuning of the CdTe/CdS core/shell QDs could only be achieved at pH 7.5 providing particles luminescing from green to red. The growth rate was accelerated at higher pH values resulting in bulk CdTe/CdS core/shell QDs in a shorter time period. Another, important observation in this study was that the pH values of the reaction solutions before DMSA addition was around 9.0 for each case. Therefore, it was concluded that this pH change mainly influenced the core yielding better quality crystals (higher QY) at lower pH values and this directly affected the QY of the core/shell QDs in the same manner.

In order to determine the conditions yielding the best luminescing particles, variables that could affect the CdTe core were studied as well. The SH(2MPA)/Cd ratio was altered because ligand concentration is also an important factor. At the optimum SH (DMSA)/Cd (initial) ratio 0.7 and initial pH 7.5, 2-MPA amount was varied by applying SH (2-MPA)/Cd (initial) ratio of 1.5, 2.4 and 5.0. Lower ligand concentrations resulted in a better luminescing CdTe core QDs (4.6% at ratio=5.0, 19.0% at ratio=2.4 and 30.5% at ratio=1.5). The best QY for CdTe/CdS core/shell was achieved at the ratio of 2.4 (73.3%) and highly green to red luminescent CdTe/CdS core/shell QDs could only be obtained at

this ratio. The ratio of 1.5 and 5.0 gave 58.4% and 38.6% QY, respectively, and color could be tuned till orange. Therefore, Cd^{2+}:Te^{2-}:SH(2-MPA)=1:0.38:1.5 was chosen as the optimum ratio for 2-MPA capped CdTe QDs but Cd^{2+}:Te^{2-}:SH(2-MPA)=1:0.38:2.4 was the best for 2-MPA capped CdTe/CdS core/shell QD synthesis.

Stability is another important parameter for these QDs. Stability, both luminescent and colloidal, of CdTe and CdTe/CdS was studied under ambient conditions and under storage in refrigerator. Both were stable in cold and dark conditions; and both has lost their colloidal stability after 2-3 weeks under ambient conditions. However, size shrinkage occurred in CdTe QDs due to the oxidation of Te^{2-} at the surface of the crystal but this situation has not appeared in CdTe/CdS confirming the formation of an effective CdS shell.

Capping of surface with the CdS also improved the luminescence lifetimes (both short and long-lifetime components) and increased the weight of the surface related long-lifetime component.

As a consequence of all these studies, CdTe/CdS core/shell QDs luminescing from green to red were accomplished with a maximum QY of 73.3% by the decomposition of DMSA at initial pH of 7.5 and Cd^{2+}:Te^{2-}:SH(2-MPA)=1:0.38:2.4 andCd^{2+}:SH(DMSA)=1:0.7. This QY value was obtained without any post-preparative method. Moreover, they are highly stable in the refrigerator in dark, so they can be stored safely for months. They are also more stable than CdTe quantum dots under ambient conditions and have longer fluorescence lifetime.

APPENDIX

CALCULATION OF QUANTUM DOT SIZE BY THE BRUS EQUATION AND ABSORBANCE SPECTRUM

Particles size of QDs is determined by a mathematical expression called "Brus Equation" proposed by L. Brus in 1984 [15]. As shown in Eqn. A.1, it is composed of three terms which are the bulk band gap energy of the semiconductor (E_g), quantum confinement energy or the kinetic energy of carriers (E_k) and Coulomb energy (E_{Coul}). Each term has been discussed in 1.2.1 in detail.

$$E_g(dot) = E_g(bulk) + E_k + E_c \tag{A.1}$$

where

$$E_g(dot) = h\upsilon_{edge} = h\frac{c}{\lambda_{edge}} \tag{A.2}$$

$$E_k = \frac{h^2}{8r^2}\left[\frac{1}{m^*_e} + \frac{1}{m^*_h}\right] \tag{A.3}$$

$$E_{Coul} = -1.8\frac{e^2}{4\pi\varepsilon\varepsilon_0 r} \tag{A.4}$$

When Eqs. (A.2), (A.3) and (A.4) are inserted in Eqn. (A:1), the following relation is obtained to be solved for size calculation:

$$h\frac{c}{\lambda_{edge}} = E_g(bulk) + \frac{h^2}{8r^2}\left[\frac{1}{m^*_e} + \frac{1}{m^*_h}\right] - 1.8\frac{e^2}{4\pi\varepsilon\varepsilon_0 r} \tag{A.5}$$

Here, the constant parameters are:

$$m_e = 9.10938188\times10^{-31} kg \tag{A.6}$$

$$\varepsilon_0 = 8.854\times10^{-12}\frac{F}{m} or \frac{C}{Vm} \tag{A.7}$$

$$h = 6.62606\times10^{-34} Js = 4.13566\times10^{-15} eVs \tag{A.8}$$

$$e = 1.602\times10^{-19} C \tag{A.9}$$

$$c = 3.0\times10^{8}\frac{m}{s} \tag{A.10}$$

Each term should be solved separately by substituting these parameters. Let us start with the band gap energy, Eg, of the nanocrystals:

$$E_g(dot) = h\frac{c}{\lambda_{edge}} = 4.13566\times10^{-15}\left[eV\cdot s\right]\frac{3.0\times10^{8}\left[\frac{m}{s}\right]\times10^{9}\left[\frac{nm}{m}\right]}{\lambda_{edge}\left[nm\right]}$$

$$\boxed{E_g(dot) = \frac{1240.7\left[eV.nm\right]}{\lambda_{edge}\left[nm\right]}} \tag{A.11}$$

There is an important point to be discussed here. The λ_{edge} term corresponds to the absorption edge in the absorption spectrum and the determination of it is illustrated in Figure A.1. A linear line is drawn at the linear region of the absorbance plot (blue line) and

the intersection point of this line with the reference region (red line) gives the absorption edge of the sample.

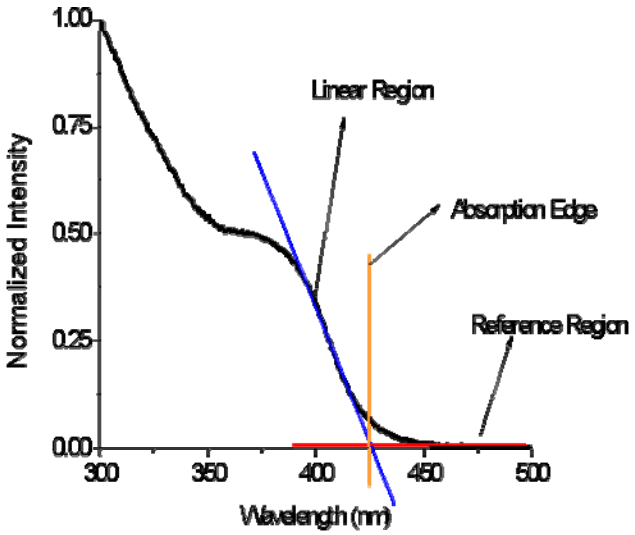

Figure A.1 Representative plot of the absorption edge determination

Since the band gap energy (Eg) is an intrinsic property of semiconductors, we will skip to the next term which is the quantum confinement energy of carriers, E_k:

$$E_k = \frac{h^2}{8r^2}\left(\frac{1}{m^*_e}+\frac{1}{m^*_h}\right) = \frac{\left(4.13566\times10^{-15}\left[eV\cdot s\right]\right)^2}{8\times\left(r\left[nm\right]\right)^2}\left(\frac{1}{m^*_e}+\frac{1}{m^*_h}\right)$$

$$E_k = \frac{2.13796\times10^{-30}\left[eV\cdot s\right]^2}{\left(r\left[nm\right]\right)^2}\left(\frac{1}{m^*_e\left[kg\right]}+\frac{1}{m^*_h\left[kg\right]}\right)\times\frac{\left[kg\cdot m^2/s^2\right]}{\left[J\right]}\times\frac{1.602\times10^{-19}\left[J\right]}{\left[eV\right]}\times\frac{\left(10^9\left[nm\right]\right)^2}{\left[m\right]^2}$$

$$\boxed{E_k = \frac{3.425\times10^{-31}\left[eV.nm^2\right]}{\left(r\left[nm\right]\right)^2}\left(\frac{1}{m^*_e}+\frac{1}{m^*_h}\right)} \qquad (A.12)$$

The last term to be solved is the Coulomb energy, E_{Coul}:

$$E_{Coul} = -1.8\frac{e^2}{4\pi\varepsilon\varepsilon_0 r} = -1.8\frac{\left(1.602\times10^{-19}[C]\right)^2}{4\times\pi\times\varepsilon\times8.854\times10^{-12}\left[\frac{C}{V\cdot m}\right]\times r[nm]}\times\frac{[eV]}{1.602\times10^{-19}[CV]}\times\frac{10^9[nm]}{[m]}$$

$$\boxed{E_{Coul} = -\frac{2.592[eV.nm]}{\varepsilon\times r[nm]}} \qquad \text{(A.13)}$$

Inserting E_g(dot) (A.11), E_g(bulk), E_k and E_{Coul} terms into Eqn. (A.1), we get an equation for the size calculation of all quantum dots and it is given as:

$$\frac{1240.7[eV.nm]}{\lambda_{edge}[nm]} = E_g(bulk) + \frac{3.425\times10^{-31}[eV.nm^2]}{r[nm]^2}\left(\frac{1}{m^*_e}+\frac{1}{m^*_h}\right) - \frac{2.592[eV.nm]}{\varepsilon\times r[nm]}$$

Since $d = 2\times r$;

$$\boxed{\frac{1240.7[eV.nm]}{\lambda_{edge}[nm]} = E_g(bulk) + \frac{1.37\times10^{-30}[eV.nm^2]}{(d[nm])^2}\left(\frac{1}{m^*_e}+\frac{1}{m^*_h}\right) - \frac{5.184[eV.nm]}{\varepsilon\times d[nm]}} \qquad \text{(A.14)}$$

A.1 CdS Particle Size Calculation

In order to calculate the size of CdS QDs, we need to know these parameters:

$m^*_e = 0.3m_e$ where $m_e = 9.10938188\times10^{-31}[kg]$
$m^*_h = 0.8m_e$

$E_g = 2.58eV$

$\varepsilon = 5.7$

When these parameters are substituted in Eqn. (A.14), the final equation belonging only to CdS QDs is as follows:

$$\boxed{\frac{1240.7[eV.nm]}{\lambda_{edge}[nm]} = 2.42[eV] + \frac{6.893[eV.nm^2]}{(d[nm])^2} - \frac{0.909[eV.nm]}{d[nm]}} \quad \text{(A.15)}$$

A.2 CdTe Particle Size Calculation

In order to calculate the size of CdTe QDs, we need to know these parameters:

$m^*_e = 0.14m_e$ where $m_e = 9.10938188 \times 10^{-31}[kg]$
$m^*_h = 0.37m_e$

$E_g = 1.50eV$

$\varepsilon = 10.6$

When these parameters are substituted in Eqn. (A.14), the final equation belonging only to CdTe QDs is as follows:

$$\boxed{\frac{1240.7[eV.nm]}{\lambda_{edge}[nm]} = 1.50[eV] + \frac{14.8[eV.nm^2]}{(d[nm])^2} - \frac{0.489[eV.nm]}{d[nm]}} \quad \text{(A.16)}$$

BIBLIOGRAPHY

1. Kroto, H.W., et al., *C-60 - Buckminsterfullerene.* Nature, 1985. **318**(6042): p. 162-163.

2. Fan, S.S., et al., Self-oriented regular arrays of carbon nanotubes and their field emission properties. Science, 1999. **283**(5401): p. 512-514.

3. Alivisatos, A.P., *Semiconductor clusters, nanocrystals, and quantum dots.* Science, 1996. **271**(5251): p. 933-937.

4. Klimov, V.I., et al., *Electron and hole relaxation pathways in semiconductor quantum dots.* Physical Review B, 1999. **60**(19): p. 13740-13749.

5. Bockelmann, U., Exciton relaxation and radiative recombination in semiconductor quantum dots. 1993, Physical Review B: Garching.

6. Brus, L.E., A Simple-Model for the Ionization-Potential, Electron-Affinity, and Aqueous Redox Potentials of Small Semiconductor Crystallites. Journal of Chemical Physics, 1983. **79**(11): p. 5566-5571.

7. Ouchi, I., et al., Excitation and emission spectra of polyethylene terephthalate and polyethylene 2,6-naphthalate films. Polymers for Advanced Technologies, 1999. **10**(3): p. 195-198.

8. Peng, X.G., et al., Epitaxial growth of highly luminescent CdSe/CdS core/shell nanocrystals with photostability and electronic accessibility. Journal of the American Chemical Society, 1997. **119**(30): p. 7019-7029.

9. Deng, D.W., J.S. Yu, and Y. Pan, *Water-soluble CdSe and CdSe/CdS nanocrystals: A greener synthetic route.* Journal of Colloid and Interface Science, 2006. **299**(1): p. 225-232.

10. Hines, M.A. and P. Guyot-Sionnest, *Synthesis and characterization of strongly luminescing ZnS-Capped CdSe nanocrystals.* Journal of Physical Chemistry, 1996. **100**(2): p. 468-471.

11. Peng, H., et al., Preparation of water-soluble CdTe/CdS core/shell quantum dots with enhanced photostability. Journal of Luminescence, 2007. **127**(2): p. 721-726.

12. Kim, S., et al., *Type-II quantum dots: CdTe/CdSe(core/shell) and CdSe/ZinTe(core/shell) heterostructures.* Journal of the American Chemical Society, 2003. **125**(38): p. 11466-11467.

13. Chen, C.Y., et al., Type-II CdSe/CdTe/ZnTe (core-shell-shell) quantum dots with cascade band edges: The separation of electron (at CdSe) and hole (at ZnTe) by the CdTe layer. Small, 2005. **1**(12): p. 1215-1220.

14. Talapin, D.V., et al., *CdSe/CdS/ZnS and CdSe/ZnSe/ZnS core-shell-shell nanocrystals.* Journal of Physical Chemistry B, 2004. **108**(49): p. 18826-18831.

15. Brus, L.E., Electron Electron and Electron-Hole Interactions in Small Semiconductor Crystallites - the Size Dependence of the Lowest Excited Electronic State. Journal of Chemical Physics, 1984. **80**(9): p. 4403-4409.

16. Brus, L., Electronic Wave-Functions in Semiconductor Clusters - Experiment and Theory. Journal of Physical Chemistry, 1986. **90**(12): p. 2555-2560.

17. Schmid, G., *Nanoparticles: From Theory to Application*. 3 ed. 2004, Weinheim: Wiley-VCH. 444.

18. Luis M. Liz-Marzán, P.V.K., *Nanoscale Materials*. 2003: Springer US. 499.

19. Demas, J.N. and G.A. Crosby, *The Measurement of Photoluminescence Quantum Yields. A Review.* J. Phys. Chem., 1971. **75**(8): p. 991-1024.

20. Murray, C.B., D.J. Norris, and M.G. Bawendi, *Synthesis and Characterization of Nearly Monodisperse Cde (E = S, Se, Te) Semiconductor Nanocrystallites.* Journal of the American Chemical Society, 1993. **115**(19): p. 8706-8715.

21. Peng, Z.A. and X.G. Peng, *Formation of high-quality CdTe, CdSe, and CdS nanocrystals using CdO as precursor.* Journal of the American Chemical Society, 2001. **123**(1): p. 183-184.

22. Bailey, R.E. and S.M. Nie, *Alloyed semiconductor quantum dots: Tuning the optical properties without changing the particle size.* Journal of the American Chemical Society, 2003. **125**(23): p. 7100-7106.

23. Talapin, D.V., et al., *A novel organometallic synthesis of highly luminescent CdTe nanocrystals.* Journal of Physical Chemistry B, 2001. **105**(12): p. 2260-2263.

24. Qu, L.H. and X.G. Peng, *Control of photoluminescence properties of CdSe nanocrystals in growth.* Journal of the American Chemical Society, 2002. **124**(9): p. 2049-2055.

25. Qu, L.H., Z.A. Peng, and X.G. Peng, *Alternative routes toward high quality CdSe nanocrystals.* Nano Letters, 2001. **1**(6): p. 333-337.

26. Gao, M.Y., et al., *Strongly photoluminescent CdTe nanocrystals by proper surface modification.* Journal of Physical Chemistry B, 1998. **102**(43): p. 8360-8363.

27. Gaponik, N., et al., *Thiol-capping of CdTe nanocrystals: An alternative to organometallic synthetic routes.* Journal of Physical Chemistry B, 2002. **106**(29): p. 7177-7185.

28. Zhang, H., et al., The influence of carboxyl groups on the photoluminescence of mercaptocarboxylic acid-stabilized CdTe nanoparticles. Journal of Physical Chemistry B, 2003. **107**(1): p. 8-13.

29. Zhang, H., et al., *Hydrothermal synthesis for high-quality CdTe nanocrystals.* Advanced Materials, 2003. **15**(20): p. 1712-+.

30. Guo, J., W.L. Yang, and C.C. Wang, Systematic study of the photoluminescence dependence of thiol-capped CdTe nanocrystals on the reaction conditions. Journal of Physical Chemistry B, 2005. **109**(37): p. 17467-17473.

31. Li, M.Y., et al., Hydrothermal synthesis of highly luminescent CdTe quantum dots by adjusting precursors' concentration and their conjunction with BSA as biological fluorescent probes. Talanta, 2007. **72**(1): p. 89-94.

32. He, Y., et al., *Synthesis of CdTe nanocrystals through program process of microwave irradiation.* Journal of Physical Chemistry B, 2006. **110**(27): p. 13352-13356.

33. Wang, Y., et al., Mechanism of strong luminescence photoactivation of citrate-stabilized water-soluble nanoparticles with CdSe cores. Journal of Physical Chemistry B, 2004. **108**(40): p. 15461-15469.

34. Bao, H.B., et al., Enhancement effect of illumination on the photoluminescence of water-soluble CdTe nanocrystals: Toward highly fluorescent CdTe/CdS core-shell structure. Chemistry of Materials, 2004. **16**(20): p. 3853-3859.

35. He, Y., et al., Microwave-assisted growth and characterization of water-dispersed CdTe/CdS core-shell nanocrystals with high photoluminescence. Journal of Physical Chemistry B, 2006. **110**(27): p. 13370-13374.

36. Wang, C.L., et al., Application of ultrasonic irradiation in aqueous synthesis of highly fluorescent CdTe/CdS core-shell nanocrystals. Journal of Physical Chemistry C, 2007. **111**(6): p. 2465-2469.

37. Gu, Z.Y., et al., One-pot synthesis of highly luminescent CdTe/CdS core/shell nanocrystals in aqueous phase. Nanotechnology, 2008. **19**(13): p. -.

38. Celebi, S., et al., Synthesis and characterization of poly(acrylic acid) stabilized cadmium sulfide quantum dots. Journal of Physical Chemistry B, 2007. **111**(44): p. 12668-12675.

39. Winter, J.O., et al., Variation of cadmium sulfide nanoparticle size and photoluminescence intensity with altered aqueous synthesis conditions. Colloids and Surfaces a-Physicochemical and Engineering Aspects, 2005. **254**(1-3): p. 147-157.

40. Henini, M. and M. Bugajski, *Advances in self-assembled semiconductor quantum dot lasers.* Microelectronics Journal, 2005. **36**(11): p. 950-956.

41. Robel, I., et al., Quantum dot solar cells. Harvesting light energy with CdSe nanocrystals molecularly linked to mesoscopic TiO2 films. Journal of the American Chemical Society, 2006. **128**(7): p. 2385-2393.

42. Costa-Fernandez, J.M., R. Pereiro, and A. Sanz-Medel, *The use of luminescent quantum dots for optical sensing.* Trac-Trends in Analytical Chemistry, 2006. **25**(3): p. 207-218.

43. Jamieson, T., et al., *Biological applications of quantum dots.* Biomaterials, 2007. **28**(31): p. 4717-4732.

44. Chan, W.C.W. and S.M. Nie, *Quantum dot bioconjugates for ultrasensitive nonisotopic detection.* Science, 1998. **281**(5385): p. 2016-2018.

45. Weng, J.F., et al., Highly luminescent CdTe quantum dots prepared in aqueous phase as an alternative fluorescent probe for cell imaging. Talanta, 2006. **70**(2): p. 397-402.

46. Green, M., et al., *A facile route to CdTe nanoparticles and their use in bio-labelling.* Journal of Materials Chemistry, 2007. **17**(19): p. 1989-1994.

47. Chan, W.C.W., et al., *Luminescent quantum dots for multiplexed biological detection and imaging.* Current Opinion in Biotechnology, 2002. **13**(1): p. 40-46.

48. Pinaud, F., et al., *Advances in fluorescence imaging with quantum dot bio-probes.* Biomaterials, 2006. **27**(9): p. 1679-1687.

49. Iyer, G., et al., *Peptide coated quantum dots for biological applications.* Ieee Transactions on Nanobioscience, 2006. **5**(4): p. 231-238.

50. Santos, J.G., et al., Magnetite-based biocompatible magnetic fluid: temperature and concentration investigation using magnetic resonance. Journal of Magnetism and Magnetic Materials, 2004. **272-76**: p. 2330-2331.

51. Fauconnier, N., et al., *Thiolation of maghemite nanoparticles by dimercaptosuccinic acid.* Journal of Colloid and Interface Science, 1997. **194**(2): p. 427-433.

52. Auffan, M., et al., In vitro interactions between DMSA-coated maghemite nanoparticles and human fibroblasts: A physicochemical and cyto-genotoxical study. Environmental Science & Technology, 2006. **40**(14): p. 4367-4373.

53. Morais, P.C., et al., Susceptibility investigation of the nanoparticle coating-layer effect on the particle interaction in biocompatible magnetic fluids. Journal of Magnetism and Magnetic Materials, 2004. **272-76**: p. 2328-2329.

54. Crisponi, G., et al., Equilibrium study on Cd(II) and Zn(II) chelates of mercapto carboxylic acids. Polyhedron, 2002. **21**(14-15): p. 1319-1327.

55. Zhu, X.F. and S.Z. Lever, Analysis of meso-2,3-dimercaptosuccinic acid in human urine by capillary electrophoresis using direct injection. Analytical and Bioanalytical Chemistry, 2003. **377**(4): p. 666-669.

56. Klemm, W., H. Sodomann, and P. Langmesser, *Beitrage zur Kenntnis der Alkalimetallchalkogenide.* 1939. **241**(Z. Anorg. Allgem. Chemie): p. 281.

57. Hayes, D., et al., *Radiolytic Production and Properties of Ultrasmall Cds Particles.* Journal of Physical Chemistry, 1989. **93**(11): p. 4603-4608.

58. Swayambunathan, V., et al., *Thiol Surface Complexation on Growing Cds Clusters.* Journal of the American Chemical Society, 1990. **112**(10): p. 3831-3837.

59. Shavel, A., N. Gaponik, and A. Eychmuller, *Factors governing the quality of aqueous CdTe nanocrystals: Calculations and experiment.* Journal of Physical Chemistry B, 2006. **110**(39): p. 19280-19284.

60. Zhang, X., et al., Preparation and optical properties of CdTe/CdO center dot nH(2)O core/shell nano-composites in aqueous solution. Chinese Journal of Chemical Physics, 2007. **20**(6): p. 779-783.

61. Rogach, A.L., et al., *Aqueous synthesis of thiol-capped CdTe nanocrystals: State-of-the-art.* Journal of Physical Chemistry C, 2007. **111**(40): p. 14628-14637.

62. Wang, X.Y., et al., Surface-related emission in highly luminescent CdSe quantum dots. Nano Letters, 2003. **3**(8): p. 1103-1106.

VITA

Esra Sevinç was born in Van, Turkey in 1984. She completed his high school in Hacı Ömer Tarman Anatolian High School in 2002. She received her B.S. degree from the Department of Chemical Engineering at Middle East Technical University (METU), Ankara in 2007. In 2007, she started her M.S. degree study in Materials Science and Engineering Department at Koç University (KU).